PEM FUEL CELL MODELING AND OPTIMIZATION USING A GENETIC ALGORITHM

by

Glenn Creighton Catlin

A thesis submitted to the Faculty of the University of Delaware in partial fulfillment of the requirements for the degree of Master of Science in Mechanical Engineering

Spring 2010

PEM FUEL CELL MODELING AND OPTIMIZATION USING A GENETIC ALGORITHM

by

Glenn Creighton Catlin

Approved: _____
Suresh G. Advani , Ph.D.
Professor in charge of thesis on behalf of the Advisory Committee

Approved: _____
Ajay K. Prasad , Ph.D.
Professor in charge of thesis on behalf of the Advisory Committee

Approved: _____
Anette M. Karlson, Ph.D.
Chair of the Department of Mechanical Engineering

Approved: _____
Michael J. Chajes, Ph.D.
Dean of the College of Engineering

Approved: _____
Debra Hess Norris, M.S.
Vice Provost for Graduate and Professional Education

ACKNOWLEDGMENTS

I would like to thank the Department of Mechanical Engineering and the Fuel Cell Research Lab as well the Federal Transit Administration for funding me throughout my graduate studies. My desire to apply mechanical engineering to renewable and sustainable energy applications was realized through the wonderful opportunity to learn and conduct research here at The University of Delaware. Thanks for funding also goes to the National Science Foundation's Solar Hydrogen IGERT program. This program offered me a unique and valuable experience to collaborate with highly motivated and truly unforgettable graduate students of various disciplines related to the solar hydrogen energy path. I had the opportunity to learn about disciplines of science and engineering as well as economic and policy issues that are related to bringing new and innovative ideas to potential real world applications.

Great thanks is given to both of my advisors: Dr. Ajay Prasad and Dr. Suresh Advani. Their expertise, combined with their consistent and thoughtful guidance, offered me an extremely valuable resource that propelled me through my research and greatly increased my understanding of PEMFCs. It is through their excellent advisement that I have been able to reach my academic goals. I would also like to extend thanks to Dr. Vic Kaliakin for taking interest in my project by becoming a member of my thesis committee and for providing me with a solid background in finite element analysis.

I would also like to thank all of the Fuel Cell Research Lab associates for their help with various stages of my project. In particular, I owe thanks to Erik

Koepf for his eagerness to help answer and ask the right questions, Doug Brunner for his general knowledge of many things and his tenacity to help solve problems that I encountered, Srikanth Arisetty for his help with numerical modeling, and Dr. Dusan Spernjak for helping me verify his experimental work.

I especially thank my parents, Marie and Creighton, as well as my sisters, Diane and Amy, for their continued support and motivation throughout all of my endeavors.

TABLE OF CONTENTS

LIST OF FIGURES . . . . . **vii**
LIST OF TABLES . . . . . **x**
NOMENCLATURE . . . . . **xi**
ABSTRACT . . . . . **xiii**

Chapter

1 POLYMER ELECTROLYTE MEMBRANE FUEL CELLS **1**

1.1 Introduction 1
1.2 Polymer Electrolyte Membrane Fuel Cell Background 2
1.3 Research Objectives 7
1.4 Thesis Overview 9

2 PEM FUEL CELL MODELING **11**

2.1 Motivation 11
2.2 Model Assumptions 13
2.3 Governing Equations 14
2.4 PEMFC Boundary Conditions and Material Properties 17
2.5 Meshing Strategy and Convergence Considerations 18
2.6 PEMFC Model Validation and Verification 20

2.6.1 Experimental Validation and Verification 20
2.6.2 Analytical and Numerical Comparison 22
2.6.3 Verification and Validation Summary 24

2.7 Chapter Summary 24

3 OPTIMIZATION METHODOLOGY AND AUTOMATION . . . 26

3.1 Genetic Algorithm Overview . . . 26
3.2 Genetic Algorithm Theory . . . 26

3.2.1 MATLAB GA Toolbox set parameters . . . 28

3.3 Communication Script . . . 29
3.4 Summary . . . 32

4 SINGLE-SERPENTINE CHANNEL OPTIMIZATION . . . 33

4.1 Introduction . . . 33
4.2 Problem Definition . . . 33
4.3 Optimization Output . . . 37
4.4 Comparison of Best and Worst individuals . . . 38
4.5 Comparison to neighbors . . . 43
4.6 Summary . . . 45

5 DOUBLE-SERPENTINE CHANNEL OPTIMIZATION . . . 50

5.1 Introduction . . . 50
5.2 Problem Definition . . . 51
5.3 Comparison of Best and Worst Individuals . . . 54
5.4 Comparison to Neighbors . . . 57
5.5 Comparison Between the Performance of the Best Single-Serpentine and Double-Serpentine Channel Configurations . . . 58
5.6 Summary . . . 60

6 CONCLUSIONS AND FUTURE WORK . . . 70
BIBLIOGRAPHY . . . 74

LIST OF FIGURES

1.1 PEMFC schematic cross section 4

1.2 General polarization curve loss regions: (i) kinetic, (ii) ohmic, and (iii) mass transport. 6

1.3 Basic PEMFC channel designs 10

2.1 Comparison of PEMFC FLUENT Add-on module simulation and experimentally determined results. 22

2.2 Comparison of numerical and analytical PEMFC pressure distribution along center pass. 23

3.1 GA Flow Chart 30

4.1 Schematic of the three-parameter single-serpentine configuration. . 34

4.2 Convergence of GA population toward the "best" individual. 38

4.3 Best and worst individuals' contour plots of current density (A/m^2) at the cathode GDL and CL interface. 40

4.4 Best and worst individuals' contour plots of oxygen concentration ($kmol/m^3$) along the cathode channel. 41

4.5 Best and worst individuals' contour plots of hydrogen concentration ($kmol/m^3$) along the anode channel. 42

4.6 Oxygen concentration ($kmol/m^3$) at the top, middle, and bottom of the cathode GDL for the best (left) and worst (right) performers. . 46

4.7 Velocity vectors (m/s) in best (top) and worst (bottom) individuals of the cathode GDL. Velocities correspond to the midplane of the GDL 47

4.8 Absolute pressure (Pa) in the cathode GDL mid-plane for the best (left) and worst (right) performers. 48

4.9 Result of a bracketing study that compares the fitness of neighbors to the fitness of the best individual. 48

4.10 Gross and net power density comparison of neighbors to best individual. 49

5.1 Schematic of the five-parameter (CL, CW_1, CW_2, LW_1, LW_2) double-serpentine configuration. 52

5.2 Schematic of the double-serpentine manifold. 53

5.3 Best (top) and worst (bottom) individuals' contour plots of current density (A/m^2) at the cathode GDL-CL interface. 55

5.4 Best (top) and worst (bottom) individuals' layered contour plots of GDL molar concentration ($kmol/m^3$) of oxygen from the cathode GDL midplane (top) to the GDL-CL interface (bottom). 61

5.5 Best (top) and worst (bottom) individuals' plots of velocity (m/s) at the cathode GDL midplane. 62

5.6 Comparison of the best double-serpentine individual's performance to that of its neighbors. 63

5.7 Current Density (A/m^2) contour plots at the cathode GDL-CL interface for the best single- (top) and the best double-serpentine (bottom) channel configurations. 64

5.8 Contour plots of oxygen molar concentration ($kmol/m^3$) at the cathode GDL midplane for the best single- (top) and the best double-serpentine (bottom) channel configurations. 65

5.9 Velocity vectors (m/s) in the cathode GDL midplane for the best single- (top) and the best double-serpentine (bottom) channel configurations at adjacent channel roots. 66

5.10 Contour plot of the Peclet number in the cathode GDL midplane of the best single-serpentine individual. 67

5.11 Contour plot of the Peclet number in the cathode GDL midplane of the best double-serpentine individual. 68

5.12 Pressure (Pa) contour plots in the cathode GDL midplane for the best single- (top) and the best double-serpentine (bottom) channel configurations. 69

LIST OF TABLES

2.1 Source Term Values 17

2.2 PEMFC Material Properties and Parameters 18

2.3 PEMFC Boundary Conditions 18

3.1 Conservation of Energy Source Terms 29

4.1 Three Parameter Search Space 35

4.2 Three-Parameter Study: Best and Worst Individuals 39

5.1 Double-Serpentine Search Space 53

5.2 Double-Serpentine Best and Worst Individuals 54

NOMENCLATURE

Symbol	Description	Units
D	diffusivity	m^2/s
F	Faraday constant	C/kgmol
h	enthalpy	J/kg
I	current	A
i	current density	A/m^2
$j_{an,cat}^{ref}$	volumetric reference exchange current density	$kgmol/m^3$
K	permeability	m^2
k	thermal conductivity	$1/\Omega \cdot m$
M	molecular mass	kg/kmol
m	dimensionless quantity	[dimensionless]
$\dot{m}$	mass flow rate	kg/s
P	Power	W
Pe	Peclet Number	[dimensionless]
p	pressure	Pa
$R_{an,cat}$	exchange current density	A/m^3
$R_{s,m}$	electrical resistance	Ω
$R_{s,m}$	volumetric transfer coefficients	$1/m^3$
r	surface to volume ratio	1/m
T	temperature	K
t	time	s
V	voltage	V
v	velocity	m/s
X	local species concentration	$kgmol/m^3$
y	mass fraction of species	[dimensionless]

Symbol	Description	Units
α	transfer coefficient	[dimensionless]
β	membrane conductivity coefficient	[dimensionless]
δ	average distance between reaction surfaces and cell center	m
γ	concentration dependence	[dimensionless]
η	activation loss	V
ε	porosity	[dimensionless]
λ	stoichiometry	[dimensionless]
μ	viscosity	kg·m/s
ρ	density	$\mathrm{kg/m^3}$
σ	electrical conductivity	$1/(\Omega \cdot \mathrm{m})$
ϕ	electrical potential	V
ω	membrane conductivity exponent	[dimensionless]

ABSTRACT

The future of the world's energy solutions requires a diverse range of ideas relating to the harvest, storage, transmission, implementation, and use of various energy sources. Ideally these sources are incorporated in a renewable and sustainable manner. An important aspect of the efficient use of limited resources is the design of efficient systems that use these resources. Hydrogen is a potential carrier of clean and renewable energy. It is therefore important to increase the efficiency of the devices that utilize hydrogen as a reactant. This project focuses on effective design of Polymer Electrolyte Membrane Fuel Cells (PEMFCs). The optimization process in this research implements a Genetic Algorithm (GA) to efficiently and effectively search the PEMFC design parameters that have significant influence on performance. This research develops and implements a method of automatic generation of parameterized channel domains that are evaluated for performance by a computational fluid dynamics (CFD) technique. The CFD calculations are conducted by the use of commercially available software from ANSYS. The software package includes GAMBIT as the solid modeling and meshing software, the solver FLUENT, and a PEMFC Add-on Module capable of modeling the relevant physical mechanisms that describe cell operation. The result of the optimization process is a set of optimal channel parameter values for single- and double-serpentine channel configurations. The optimal values for these parameters are identified for a PEMFC of a desired nominal area.

Chapter 1

POLYMER ELECTROLYTE MEMBRANE FUEL CELLS

1.1 Introduction

Modern society depends heavily on an abundant and reliable source of energy. Ideally, the consumed consumed energy should have a minimal negative impact on the environment. There is no single answer that addresses the future demand of the world's energy requirements, but there are currently many fields dedicated to accomplishing parts of this important task. The solutions required to bring the required amount of energy to the world is a complex set of engineering problems and requires joint efforts of many scientific and engineering disciplines as well as economic and political policy integration to bring new and promising technologies into significant real-world applications. These observations offer the motivation for the work described in this thesis.

The sun is the primary source of clean and renewable energy and collecting it in as many ways possible will reduce the dependence on finite sources of energy. This energy can be collected directly by means of photovoltaic systems and solar-thermal chemical cycles or indirectly by wind turbines and tidal current collectors. The energy must either be used immediately or stored for later use. Energy storage is accomplished either by charging batteries or by converting the energy into another form for later use. Using energy to create hydrogen is a means to store large quantities of energy for later use. An important area of study is in making efficient use of the stored hydrogen. One way that the energy is converted back into

electricity is through a device known as a polymer electrolyte membrane fuel cell. It is therefore the focus of this thesis to help make effective use of the hydrogen that is delivered to the fuel cell.

1.2 Polymer Electrolyte Membrane Fuel Cell Background

A polymer electrolyte membrane fuel cell or proton exchange membrane fuel cell (PEMFC) is a device that converts chemical energy directly into electrical energy. The focus of this research will be on PEMFCs using hydrogen and oxygen as the chemical reactants. The hydrogen is supplied from an attached storage tank while the oxygen can be supplied by ambient air, although there are certain applications which require a pure oxygen supply. The electrical energy that results from the chemical reaction can be used externally by an applied load or can be included as part of a hybrid system where the produced energy is stored for later use.

The main components of a PEMFC are assembled in a layered configuration. A schematic diagram of a general PEMFC cross section is shown in Figure 1.1; it is important to note that the thicknesses of the layers in the figure are not to scale. Beginning from the outside of the cell and working in, the anode and cathode terminals are the outermost layers of the cell. These layers are known as the bipolar plates and are typically made of graphite, composites, or stainless steel for considerations of cost, structural rigidity, thermal conductivity, and electrical conductivity. The inner surface of each bipolar plate features gas flow channels which distribute the reactant gases to the inner layers of the fuel cell. Ribs located between adjacent channels are responsible for making electrical contact with the gas diffusion layer (GDL), which is the next layer as the center of the cell is approached. The surface of the ribs that makes contact with the GDL is known as the land area. The GDL is made of a thin (0.2 to 0.3 mm) porous carbon paper and serves the purpose of evenly distributing the reactants to the catalyst layers while also creating electrical contact between the catalyst layers and the land regions of the bipolar plates. The

permeability of the GDL and its effect on performance has been investigated by Pharoah [11] and Feser et al. [2].

The next layer of the cell is known as the membrane electrode assembly (MEA) and can be broken into three separate layers. The middle of the three layers is the proton exchange membrane. The unique properties of this membrane are crucial for the functionality of a fuel cell; the membrane allows the flow of protons, but resists the flow of the electrons which are instead forced to flow through the external circuit. The catalyst layers are coated on either side of the membrane and serve as the sites for the oxidation (anode) and reduction (cathode) reactions. The anode is supplied with hydrogen, and the cathode is supplied with oxygen, usually from air. The catalyst of a PEMFC is a porous carbon-supported platinum nano-particle coating that offers a relatively large surface-to-volume ratio. The high surface-to-volume ratio increases the number of available reaction sites, which can increase the resulting power density of a given cell. The water produced by the cathode catalyst layer, either in vapor or liquid form, flows through the GDL and into the channel for removal from the cell.

The cell, as described, is compressed and held together by tightening bolts that penetrate through all of the layers. The stiffness of the bi-polar plates helps to assure that the intermediate layers receive uniform compression. The compression of the cell prevents reactants from leaking out around the edges of the cell and between the layers of the cell without damaging the fragile membrane between the bipolar plates. The uniformity of the compression helps to ensure uniform thermal and electrical conductivity and flow resistance through the diffusion layers.

The following half-cell reactions take place on the anode and cathode catalyst layers, respectively:

$$\mathrm{H_2} \rightarrow 2\mathrm{H^+} + 2e^- \tag{1.1}$$

$$\frac{1}{2}\mathrm{O_2} + 2\mathrm{H^+} + 2e^- \rightarrow \mathrm{H_2O} \tag{1.2}$$

Under ideal conditions, this process proceeds continuously until either the external circuit is disconnected or the reactant gases are no longer available. Although the ideal voltage for this type of fuel cell is 1.23 V, various loss mechanisms reduce the practical operating voltage to about 0.6 V. The optimum point of operation of a particular cell is determined by examining its polarization and power curves. A polarization curve for a particular cell is constructed by operating the cell while stepping down its voltage from the open circuit voltage (OCV) in uniform steps while monitoring the resulting current produced by the cell. The output current of the cell is normalized by the nominal area of the cell for calculation of the current density. The current density is a useful metric for comparing cells of different magnitudes.

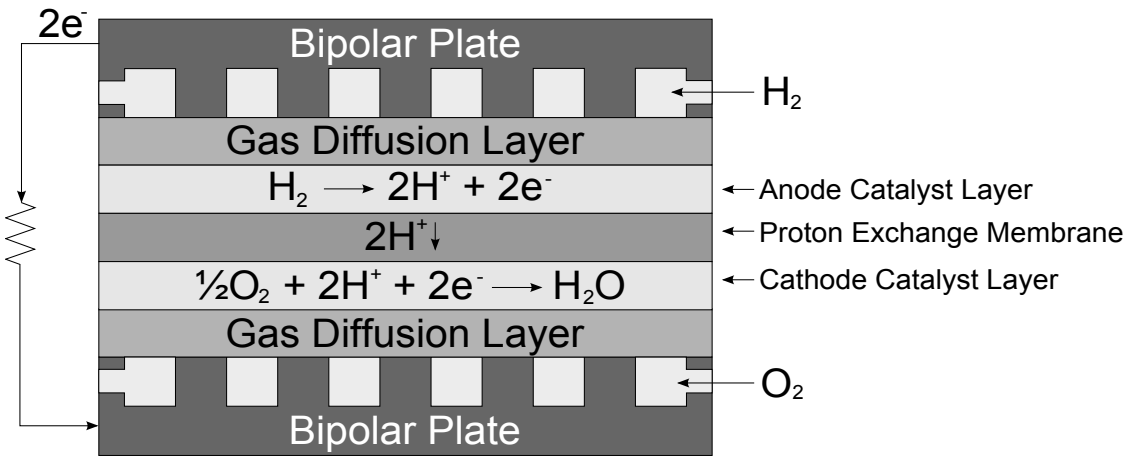

Figure 1.1: PEMFC schematic cross section

Figure 1.2 shows the schematic of a general polarization curve. The curve can be divided into three sections where each section is dominated by a different type of voltage loss mechanism. Each loss mechanism dominates in its own specific current draw regime, so it is important to understand these losses to optimize the desired operating conditions of a cell. The power density curve is constructed by

multiplying the current density by the voltage and plotting it against voltage.

Region (i) of the polarization curve is dominated by activation loss, which is a result of slow reaction kinetics. This type of loss can be reduced by using more effective catalysts, increasing the catalyst loading, increasing the operating temperature, or increasing the reactant concentration of O_2 at the inlet. Region (ii) is dominated by ohmic losses. These losses are associated with the electrical resistance of the bipolar plates and various interconnects, and the resistance to proton flow in the membrane of the cell. They can be reduced by using materials with high electrical conductivity, making sure that adjacent layers make sufficient electrical contact, maintaining electrolyte hydration, and making the electrolyte as thin as possible while ensuring that there is no electrical short between the electrodes. Region (iii) is known as the mass transport loss region. For a PEMFC, this loss is typically associated with the cathode side; the inlet air is comprised of only about 20% O_2 and can be depleted before the flow reaches the outlet of the cell for low stoichiometries. Higher stoichiometries can help to increase the amount of O_2 available for reaction, but also results in higher parasitic losses due to the increased power demand on the air compressor. Another reason for mass transport losses at high current densities is flooding due to the production of large quantities of liquid water which can saturate the gas diffusion layer and block reactant access. With the different types of loss mechanisms identified, appropriate materials selection and design recommendations for different types of operating conditions can be made. However, fuel cells often operate near region (iii) of the polarization curve, making it important to minimize all types of losses.

In this thesis, the focus is on the design of the bipolar plates of the cell. These plates are responsible for the delivery of the reactants to the catalyst layers, which is especially important on the cathode side of a cell. As previously mentioned, the oxygen is provided from ambient air and constitutes only an approximate 20%

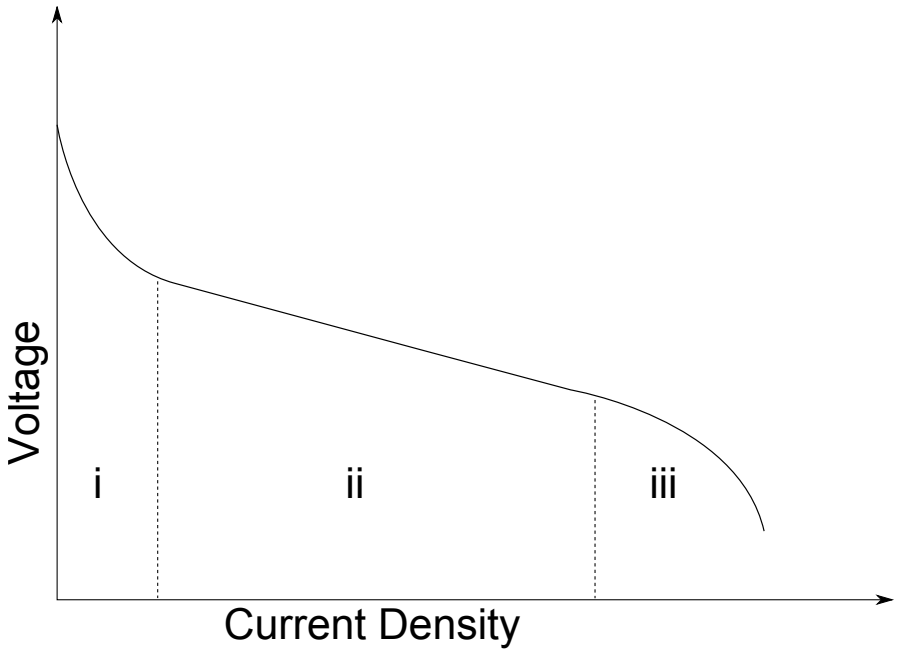

Figure 1.2: General polarization curve loss regions: (i) kinetic, (ii) ohmic, and (iii) mass transport.

of the mass flow. It is therefore important to ensure that the catalyst layer has effective access to oxygen. Otherwise, the reaction would be O_2 limited and certain regions within the cell might produce low current, resulting in poor performance. The design of the channels in the bipolar plates directly impacts a cell's ability to deliver reactants to the catalysts. A large focus on channel design can be found in the literature. The basic channel designs are shown in Figure 1.3. While some designs can be categorized by name, there is a wide variety of channel designs that do not fall into the specific categories discussed here. Referring back to Figure 1.3, each channel design has its own strengths and weaknesses. Parallel channels have reduced supply pressure requirements, but since the pressure drop across the length of the channels is small, they can easily become clogged by water and regions of the cell become incapable of producing current. Interdigitated channels are more

effective with water removal and have enhanced convective bypass into the GDL [3], but require higher operating pressures since the inlet and outlet are not directly connected by the channels. The serpentine design is a very common design, see Shimpalee et al. [7], because it has the strengths of both the previously mentioned designs. The supply pressure requirement is higher than a parallel design because the overall channel length is longer. The large pressure difference between adjacent channels enhances convective flow into the GDL and increases the amount of reactant delivery to the catalyst layer. This delivery mechanism is also known as convective bypass [3]. The serpentine design is also effective at clearing excess water from the cell, thereby reducing the problem of channel flooding. In general, increasing the convective bypass increases the performance of the cell due to the more effective reactant transport.

1.3 Research Objectives

Within each type of channel design are the parameters which describe the path that the channel takes and further impact the performance. These parameters can include, but are not limited to, the channel width, channel height, land width, and channel length. The selection of the values for these parameters have been the subject of many research investigations and have been explored experimentally, numerically, and analytically. It is important to determine how these parameters influence fuel cell performance in order to design efficient fuel cells. A study on land-to-channel width ratio was done by Yan et al. [16]. Tapering the width continuously between the inlet and outlet was investigated by Yan et al. [10]. Zhao et al. [17] developed a convection-enhanced serpentine flow field (CESFF) by forcing a single channel to double back on itself. The design results in greater pressure differences between adjacent channels than a single serpentine configuration, hence the enhanced convective bypass. All of these examples identify the parameters that are good for a cell of specific dimensions and tend to generalize that these parameters

can be used to design fuel cells of greater dimensions. It is the goal of this work to devise a method that can rapidly optimize the design of a flow field that maximizes the net power output for a specifically targeted area.

The voltage produced by a single cell is usually not sufficient for practical applications. Higher voltages are obtained by stacking multiple cells together in series. The voltage of an assembled stack is proportional to the number of cells in the stack. By evaluating the performance of a single cell, accurate predictions can be made of how a stack of the cells would perform.

Material selection as well as high-precision construction, when coupled with strategic design, can help to maximize the power output of a given cell. Therefore, it is important to choose the optimal parameters used to design a cell for a specific application. PEMFCs are typically considered good candidates for automotive and stationary power applications. These applications have different operating conditions which result in different design criteria. Therefore, it is necessary to tailor a cell's design to its specific application in order to maximize its net power output.

Specifically, the scope of this work is to use the reactant flow channel design parameters to maximize a fuel cell's performance. Fuel cells utilize expensive materials whose costs increase rapidly with an increasing nominal area of the cell. Therefore, designing a cell to make highly effective use of a given nominal area is an area of study that can help to fix material cost while increasing performance. This thesis outlines the optimization methodology that uses channel geometry as the means to increase fuel cell performance. The optimization method employs a genetic algorithm to efficiently and effectively determine optimal geometrical values within a relatively large search space. The effectiveness of a specific fuel cell is evaluated by a fitness function whose value is calculated to be net power per unit area, or net power density. The investigated channel designs include both single- and

double-serpentine configurations. A set of in-house scripts was developed to combine the strengths of finite element analysis (FEA) with a parameterized solid model drawing script and a genetic algorithm optimization method. The channel designs are targeted at a specific nominal area and set of operating conditions. The valuable contribution of this project is in the automated method of effectively determining how to best design a specifically sized PEMFC.

1.4 Thesis Overview

The goal of this project is to maximize the net power output of a polymer electrolyte membrane fuel cell by optimizing the geometric parameters of serpentine flow channels for a given cell size. A commercially available numerical model is used to conduct extensive fuel cell simulations and evaluate its performance. A detailed description of the numerical model is presented in Chapter 2. The channel design optimization is performed by implementing a Genetic Algorithm (GA) with an appropriate fitness function as described in Chapter 3. Flow channels for one application may not be optimal for other applications, so it is important to design the flow channels to suit a particular set of operating conditions. Chapter 4 will therefore use the optimization method to identify the optimal values of three design parameters that describe a single serpentine flow channel design. In Chapter 5 the complexity of the serpentine channel design is increased to allow for greater design flexibility. Specifically, the performance of a novel double-serpentine channel configuration is investigated. Chapter 6 offers a summary and discussion of the major findings of this work and identifies potential research extensions of this project.

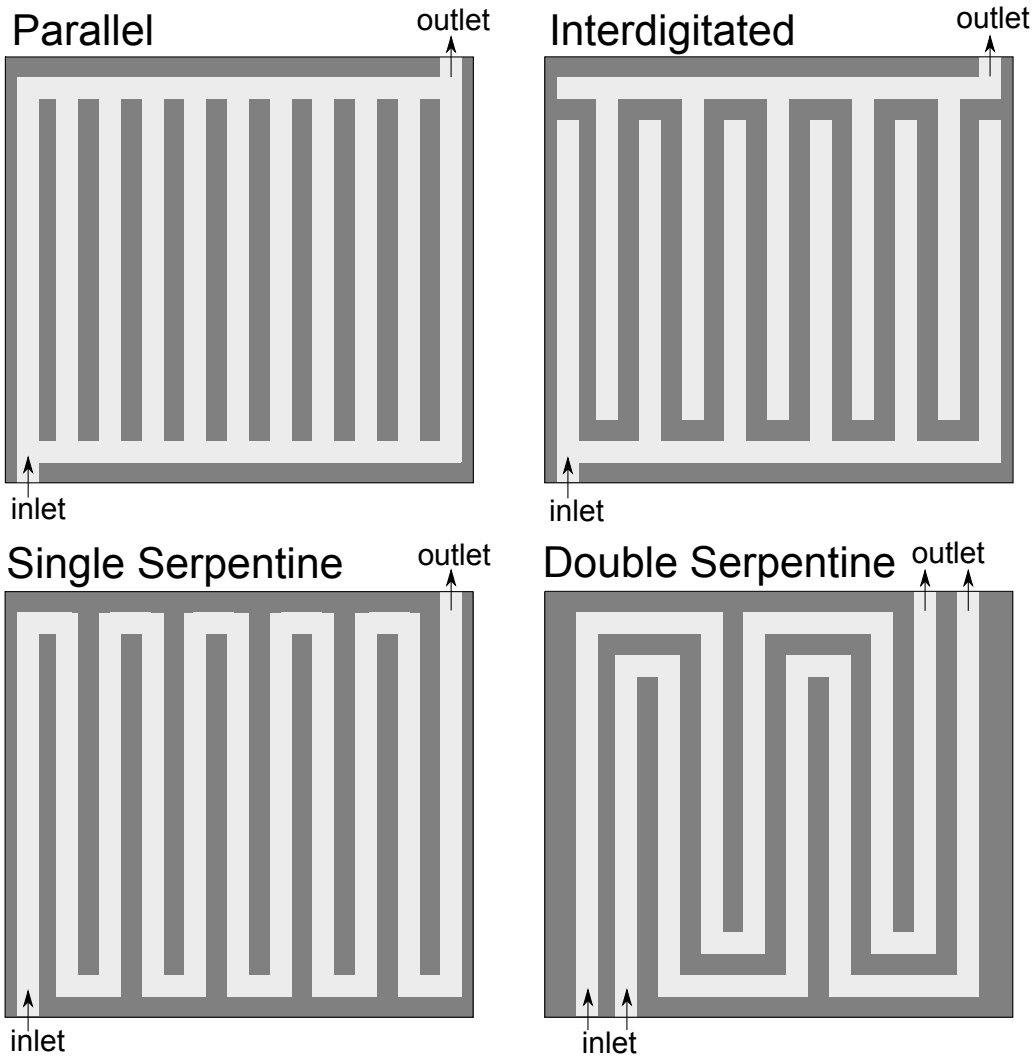

Figure 1.3: Basic PEMFC channel designs

Chapter 2

PEM FUEL CELL MODELING

2.1 Motivation

In order to evaluate the performance of a PEMFC, it is important to accurately test a cell under a specified range of conditions. The process of testing a laboratory-scale fuel cell requires the device not only to be fabricated and constructed but also requires a supply of reactants as well as a place to safely store and use them. In addition, equipment is also necessary to operate, control, and collect data from the cell. This system requires compressors, heaters, humidifiers, various interconnects, hoses, computers, sensors, and computerized data acquisition. In some cases, it is possible to use a fuel cell test stand, which is a self-contained fuel cell control station. This system is costly and requires laboratory training and resources. Even when such a suitably equipped laboratory is available, it is time-consuming and labor intensive to physically test fuel cell performance across a range of materials and architectural designs such as membranes, catalyst loading, gas diffusion layers and bipolar plate configurations, as well as for a range of operating temperatures, pressures and humidities. In order to minimize the costs associated with the design and optimization of an individual cell, it is valuable to attain predictive capability to design a cell with good performance potential before actual constructing and testing. It is therefore beneficial to include numerical modeling in the PEMFC design process.

Computer modeling and simulation are effective tools for reducing the cost and laboratory time associated with physical testing. Although some simulations

can be lengthy, the associated cost is only in the computational resources. A validated and reliable computer model is extremely efficient at evaluating a wide variety of different designs without additional hardware and software costs. The accuracy of a model is therefore an extremely important factor when deciding on the means to predict fuel cell performance. Many works have been dedicated to the construction of numerical models that can accurately predict PEMFC performance. These models have increased in complexity over time, evolving from two-dimensional models by Chen et al. [1], to relatively complex three-dimensional models. Such complex models have been created by different groups including Zhou et al. [9] who included multiphase flow, Shimpalee et al. [7], and Fan et al. [4]. These researchers have constructed their own in-house CFD models. The strength of constructing a model in-house is in the ability to have control over exactly those parts of a fuel cell are to be modeled with appropriate equations. However, we chose to use a commercially available software package (FLUENT 6.3.26) for reasons stated next.

FLUENT [6]is a powerful computational fluid dynamics (CFD) tool that enables complex fluid flows, heat transfer, and reaction kinetics to be solved in a user-friendly manner. While FLUENT alone is capable of solving the equations required to model a PEMFC, these equations must first be determined and compiled as user-defined functions. The potential for PEMFCs to become viable in the marketplace led FLUENT to include all of the relevant equations in a PEMFC Add-on Module. Therefore, the PEMFC model developed by ANSYS is used in this research and its features and capabilities are the subjects of this chapter.

These models have been used previously to investigate the influences of different material properties as well as design parameters on the power output of the PEMFC. While these models are created to accurately predict performance, there are always assumptions that are made that simplify the model. This model does not take into account areas of importance such as material degradation, the presence of

impurities in the reactant supply streams, and non-ideal operating conditions such as variances in control system responses and the non-isothermal nature of the environment which the fuel cell is bound to experience during operation. Each of those factors would lead to reduced fuel cell performance.

For the purposes of this work as well, such non-ideal operating conditions and material factors will be ignored. Because these issues will exist in any fuel cell, one can be satisfied that relying on relative performance values will be enough to provide confidence that each model's prediction is valuable. For the next section, the focus will be to demonstrate that the model is capable of accurately predicting the performance of a PEMFC. Specifically, the experimental work done in the Fuel Cell Research Lab at the University of Delaware by Spernjak et al. [13] will be used to verify the PEMFC model's results.

This chapter will simultaneously accomplish the tasks of verification and validation of the model described below as well as the script responsible for building the model. Once it is shown that the model can generate sensible and accurate results, it can be trusted as a reliable tool to create and evaluate fuel cells of varied single serpentine configurations which is the overall research goal as stated in Chapter 1. A complete description of the script that constructs these models will follow the description of the PEMFC model.

2.2 Model Assumptions

The PEMFC model used in this research is based on the following assumptions:

- The flow is laminar.
- The fluid is incompressible.
- The inlet gases follow the ideal gas law.

- The gas diffusion layers, catalyst layers, and membrane layer are isotropic materials.
- Steady state conditions exist.

2.3 Governing Equations

The reactant transport is strongly influenced by the geometry of the reactant flow channels in a PEMFC and is modeled using the conservation of mass equation found in Equation 2.1.

$$\frac{\partial \rho}{\partial t} + \nabla \cdot (\rho \mathbf{v}) = S_m \tag{2.1}$$

This equation is valid for mass balance in the channels as well as the gas diffusion layers where fluid flow and diffusion are important. The operator ∇ represents the partial derivative in Cartesian coordinates and is defined as $\frac{d}{dx}\mathbf{i} + \frac{d}{dy}\mathbf{j} + \frac{d}{dz}\mathbf{k}$. The remaining terms in the equation are as follows: ρ is the scalar density, $\mathbf{v}$ is the velocity vector, and S_m is the mass source term. For all zones in this model, $S_m = 0$.

The momentum equation is shown in Equation 2.2 and is used to solve for the fluid velocities in the channels and the GDL and the species' partial pressures.

$$\frac{\partial \rho \mathbf{v}}{\partial t} + \nabla \cdot (\rho \mathbf{v}\mathbf{v}) = -\nabla p + \nabla \cdot \tau + S_M \tag{2.2}$$

The momentum source term, S_M, is zero in all zones except for the gas diffusion layers and the catalyst layers. In these zones, Equation 2.3 defines the S_M source term and K is the permeability of the particular zone.

$$S_M = -\frac{\mu}{K}\varepsilon \mathbf{v} \tag{2.3}$$

It also is important to include the effects of temperature variation throughout a fuel cell. This task is accomplished by including the energy equation whose general form is as follows in Equation 2.4.

$$\frac{\partial}{\partial t}[\varepsilon \rho h + (1-\varepsilon)\rho_s h_s] + \nabla \cdot (\rho \mathbf{v} h) = \nabla \cdot \left(k_{eff} \nabla T - \sum_j h_j J_j \right) + S_h \tag{2.4}$$

The first two terms on the right hand side of Equation 2.4 are the conduction and species diffusion terms, respectively. S_h is the volumetric source term and is defined for all zones of the cell by Equation 2.5. In this equation, I^2R_{ohm} is the ohmic heating term, $h_{reaction}$ is the heat of formation of water term, ηR is the electric work term, and h_{phase} is the latent heat of water term.

$$S_h = I^2R_{ohm} + h_{reaction} + \eta R_{an,cat} + h_{phase} \tag{2.5}$$

The additional terms introduced by the energy equation are as follows: h is the enthalpy of the gas mixture, J is the diffusive flux, the $[\ ]_j$ subscript represents the chemical species of the bracketed quantity and the $[\ ]_s$ subscript represents the solid phase of the bracketed quantity. Zones with solid phases include the GDL, CL, membrane, and the bipolar plate. The effective thermal conductivity is calculated as follows in Equation 2.6.

$$k_{eff} = \varepsilon k_f + (1 - \varepsilon)\, k_s \tag{2.6}$$

where the subscripts $[\ ]_f$ and $[\ ]_s$ represent the fluid and solid of a specific zone, respectively. The heterogeneous reactions that take place on the catalyst surfaces are balanced by its rate of production as described below by Equation 2.7.

$$\frac{\rho D_j}{\delta}\left(y_{j,surf} - y_{j,cent}\right) r = \frac{M_{w,j}}{nF} R_{an,cat} \tag{2.7}$$

In this equation ρ is the density, $M_{w,j}$ is the molecular mass of the respective species, D_j is the mass diffusivity of species j, r is the surface-to-volume ratio of the platinum particles, $y_{jsurf,cent}$ are the mass fractions of the species at the reacting surface and cell center, respectively, and δ is the average distance between the reaction surface and cell center.

The conservation of species is required to calculate the mass balance for each of the involved reactants in this model and is defined below in Equation 2.8.

$$\frac{\partial\left(\varepsilon\rho y_j\right)}{\partial t} + \nabla\cdot\left(\rho\mathbf{v}y_i\right) = \nabla\cdot\left(\rho D_j \nabla y_j\right) + S_j \tag{2.8}$$

The effective mass diffusivity is calculated according Equation 2.9 [15, 14].

$$D_j = \varepsilon^{1.5} \left(1 - s\right)^{r_s} D_j^o \left(\frac{p_0}{p}\right)^{\gamma_p} \left(\frac{T}{T_0}\right)^{\gamma_t} \tag{2.9}$$

The species source terms, S_j, are zero except for the fluid zones and are described below in Equations 2.10 - 2.12.

$$S_{\mathrm{H}_2} = -\frac{M_{w,\mathrm{H}_2}}{2F} R_{an} \tag{2.10}$$

$$S_{\mathrm{O}_2} = -\frac{M_{w,\mathrm{O}_2}}{2F} R_{cat} \tag{2.11}$$

$$S_{\mathrm{H}_2O} = -\frac{M_{w,\mathrm{H}_2O}}{2F} R_{an} \tag{2.12}$$

The electrochemistry modeling begins with calculating the rate of hydrogen oxidation and the rate of oxygen reduction. These processes take place in the anode and cathode catalyst layers, respectively, which are deposited on opposite surfaces of the membrane layer. The following are the two potential equations solved in the PEM model. Equation 2.13 is solved for the electron transport through the solid conducting regions including the bi-polar plates, gas diffusion layers and catalyst layers. Equation 2.14 is solved for the proton conductivity through the membrane.

$$\nabla \cdot \left(\sigma_s \nabla \phi_s\right) + R_s = 0 \tag{2.13}$$

$$\nabla \cdot \left(\sigma_m \nabla \phi_m\right) + R_m = 0 \tag{2.14}$$

In the preceding equations, σ_s is the electrical conductivity of the respective solid zone, σ_m is the membrane electrical conductivity calculated by Equation 2.15 [14], ϕ is the electric potential, and R is the volumetric transfer current.

$$\sigma_m = \beta\varepsilon \left(0.514\lambda - 0.26\right)^{\omega} e^{1268\left(\frac{1}{303} - \frac{1}{T}\right)} \tag{2.15}$$

Table 2.1 summarizes the values of each source term in the appropriate computational zone. The source terms for the unnamed zones are assumed to be equal to zero.

Table 2.1: Source Term Values

Source Term	Anode	Cathode
R_s	$-R_{an}$	$+R_{cat}$
R_m	$+R_{an}$	$-R_{cat}$

The terms R_{an} and R_{cat} are defined according to the Butler-Volmer Equation as shown below in Equations 2.16 & 2.17.

$$R_{an} = j_{an}^{ref} \left(\frac{X_{\mathrm{H_2}}}{X_{\mathrm{H_2}}^{ref}} \right)^{\gamma_{an}} \left(e^{\alpha_{an} F \eta_{an}/RT} - e^{-\alpha_{cat} F \eta_{an}/RT} \right) \tag{2.16}$$

$$R_{cat} = j_{cat}^{ref} \left(\frac{X_{\mathrm{O_2}}}{X_{\mathrm{O}^r ef}} \right)^{\gamma_{cat}} \left(-e^{\alpha_{an} F \eta_{cat}/RT} + e^{-\alpha_{cat} F \eta_{cat}/RT} \right) \tag{2.17}$$

The local surface overpotentials are solved using Equations 2.18 - 2.19.

$$\eta_{an} = \phi_s - \phi_m \tag{2.18}$$

$$\eta_{cat} = \phi_s - \phi_m - V_{OC} \tag{2.19}$$

The activation loss, η, is calculated as the difference between the solid and membrane potentials as shown above in Equations 2.18 - 2.19.

2.4 PEMFC Boundary Conditions and Material Properties

This section summarizes the boundary conditions and material properties that are constant in each of the simulations that are performed on a PEMFC in this project. The inlet gases are set at a constant mass flow rate of humidified hydrogen (anode side) and air (cathode side). The mass flow rates are calculated for a stoichiometry of $\lambda = 2$ at 1 A/cm^2. Using this condition, appropriate values for the mass fluxes are calculated based on the area of a given cell. The outlet of each channel is open to the atmosphere and set to 1 atm. The cathode terminal wall is set at a constant 0.6 V and the anode terminal wall is grounded at 0 V, both terminal wall surfaces are set to 80°C. Tables 2.2-2.3 summarize the material properties and boundary conditions employed in this PEMFC model.

Table 2.2: PEMFC Material Properties and Parameters

Property	Value	Property	Value
$c_{p;col,cl,gdl}$	871 J/(kg · K)	$\alpha_{an,cat}$	2
$c_{p;mem}$	2000 J/(kg · K)	β	1
D_j^o	3×10^{-5} m^2/s	$\gamma_{an,cat}$	1
F	9.65×10^7 C/kgmol	γ_p	1.0
h_{GDL}	0.25 mm	γ_t	1.5
h_{Cl}	12.5 μm	$\varepsilon_{cl,mem}$	0.5
h_{MEM}	25 μm	$\rho_{col,cl,gdl}$	2719 kg/m^3
j_{an}^{ref}	5×10^9 A/m^3	ρ_{mem}	1980 kg/m^3
j_{cat}^{ref}	4×10^9 A/m^3	$\sigma_{cl,gdl}$	5000×10^7 1/ (ohm · m)
$k_{col,cl,gdl}$	8.0 W/(m · K)	σ_{col}	1.0×10^6 1/ (ohm · m)
$K_{gdl,cl}$	1×10^{-12} m^2	σ_{mem}	1.0×10^{-16} 1/ (ohm · m)
M_m	1100 kg/kmol	ω	1
p_o	101.325 kPa		
r	4×10^9 1/m		
T_o	300 K		
$X_{j,ref}$	1		

Table 2.3: PEMFC Boundary Conditions

Location	Boundary Condition Type	Value
Cathode and Anode Inlets	Mass Flow Rate	[calculated]
Anode and Cathode Outlets	Pressure	101325 Pa
All Exterior Surfaces	Temperature	353 K
Cathode Terminal Surface	Voltage	0.6 V
Anode Terminal Surface	Voltage	0.0 V

2.5 Meshing Strategy and Convergence Considerations

Building a three-dimensional solid model with an appropriately constructed mesh is an important concern when performing any type of numerical modeling and simulation routine. The mesh that approximates the physical model of the PEMFC should be dense enough to ensure that the solution is independent of the grid density, but also coarse enough to keep the computational power requirements to a minimum. Therefore, when designing the mesh, it is important to conduct what is known as a mesh refinement study. The mesh used in this project corresponds

to the best practice recommendations of the FLUENT PEMFC Add-on Module. Each zone of the cell requires a specific set of meshing rules. The GDL thickness if divided into 10 mesh layers, the catalyst layer thickness and membrane thicknesses are divided into four mesh layers, and the channel height is divided into 10 layers. The bends of each serpentine pass have the highest velocity and pressure gradients, so it is important to keep the mesh density high in these zones, but the mesh density is allowed to coarsen by a symmetric 1.1 meshing ratio along each pass. The result is that the channel ends are defined by cube shaped mesh elements, while the channel lengths are defined by slightly elongated hex elements. An important feature of the meshing process used by the Gmesh script ensures that there are no skewed elements. All meshed elements are hexagonal with 90 degree angles between each face.

The solver is based on the finite volume method and employs a pressure based solver with double-precision. The convergence of the model is dependent on several constraints. First, the residual quantities all must attain a tolerance at or below 1×10^{-4}. The residuals include continuity, three velocity components, energy, hydrogen species, oxygen species, water species, electrical potential, protonic potential, and water content. It is also important to monitor the quantities of interest for solution convergence. The convergence criteria therefore also require the cathode y-current density average on the cathode and the pressure at the cathode inlet to not change beyond 1×10^{-6}. These two quantities are required for calculation of the parasitic power requirements and the gross power density of each cell. These parameters comprise the fitness function for a specific cell and will be discussed in detail in Chapter 4.

This project requires multiple simulations with varying geometrical characteristics for the flow channels. Varying the channel geometry requires the construction

of a unique model and mesh for each simulation. Therefore, an efficient and methodical way of constructing and meshing a wide variety of PEMFCs is required for this study. Based on the input of geometrical parameters, a wide range of PEMFC models can easily be constructed. However, drawing and meshing each unique cell would require a prohibitively large amount of time and therefore, the process was automated using a GAMBIT journal file, which will be referred to hereon as the Gscript file. GAMBIT [5] is a commercially-available software package that was used in this study to draw the domain of a PEMFC, divide the model into a discretized mesh, and identify the necessary boundary conditions and zones. GAMBIT outputs a mesh file that can be read by FLUENT to perform a simulation at the desired operating conditions.

For the case of a single-serpentine flow field design, there are four parameters that are needed to fully describe the design for a fixed area: channel width (CW), channel height (CH), land width (LW), and cell length (L). The gscript file receives these quantities as input parameters and appropriately constructs the solid model. However, in this study, the CH is set to a constant value of 1.0 mm.

The mesh density in the thickness direction of the cell needs to be higher than along the channel length direction. In addition, the flow around the U-shaped bends at the end of each channel encompass the areas of the domain that have the highest velocity gradients, and therefore, require a higher mesh density than along the mid-section of each channel length. It is therefore possible to coarsen the mesh density along the channel length without losing accuracy in the solution.

2.6 PEMFC Model Validation and Verification

2.6.1 Experimental Validation and Verification

In order to simultaneously provide validation and verification of the model described above, a comparison to an experimental result is provided in this section. The model is constructed to replicate the cell employed by Spernjak et al. [13]. The

10 cm^2 PEMFC bipolar plates are made of graphite with a single-serpentine channel configuration. The channels are 0.8 mm wide, 1 mm high, and the land width is 0.8 mm. Humidified air is supplied at a rate of 0.18 slpm and humidified hydrogen is supplied at 0.076 slpm. The cell is set to operate at a constant 80°C. The OCV for this verification run is set to 0.778 V to match the corresponding experimental value. The simulation was initiated by setting the voltage to OCV and then the voltage was stepped down in 0.5 V decrements corresponding to the experimental data. Figure 2.1 shows a good agreement between the experimental and numerical results. It should also be noted that there are no oscillations in absolute pressure between adjacent computational nodes. This characteristic indicates that there are no compressibility issues relating to the model assumption of incompressible flow in the domain.

In addition, a check to make sure that the global conservation of mass is observed helps to verify the model. This check is accomplished by using using data output from FLUENT for one of the points on the polarization curve. For this calculation the simulation associated with the operating voltage of 0.624 V was selected. FLUENT calculates the amount of oxygen consumed by the cell and the average current flux magnitude in the y-direction at the cathode terminal wall. Using Equation 2.20 and the oxygen consumed, the total release of electrons is calculated. M is the molecular mass of oxygen, F is the Faraday constant, and $dotm$ is the oxygen consumption rate.

$$I = \frac{\dot{m}_{O_2} 4F}{M} = \frac{(6.629 \times 10^{-7})\,(4)\,(9.6485 \times 10^{7})}{31.9988} = 7.995 \text{ A} \tag{2.20}$$

Next, integrating the Current density over the cathode terminal surface results in a current of 7.993 A, which shows very good agreement for a global conservation of mass.

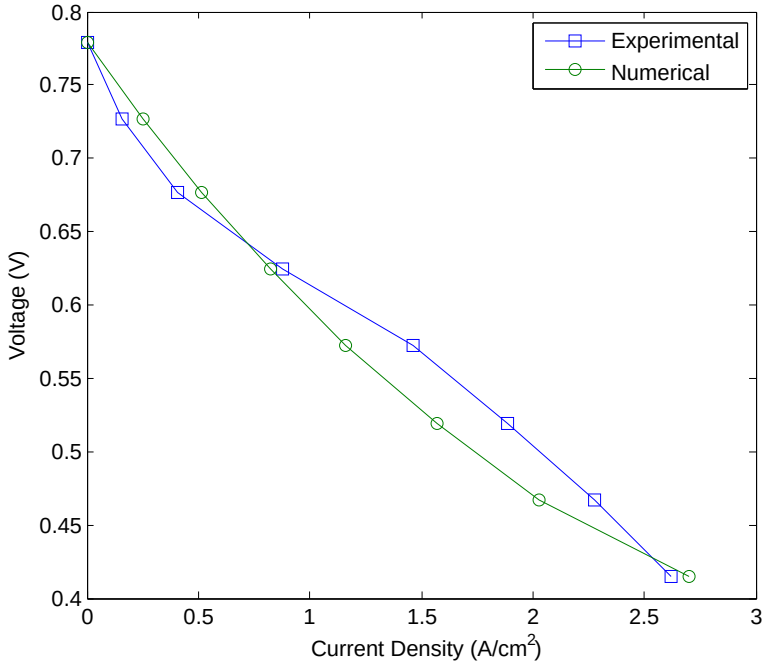

Figure 2.1: Comparison of PEMFC FLUENT Add-on module simulation and experimentally determined results.

2.6.2 Analytical and Numerical Comparison

Another important point of comparison is to investigate the flow calculations within the cell. Although the experimental verification shows that the model is capable of predicting overall performance values in the form of current density output versus voltage, it is necessary to further analyze detailed results internal to the cell. Feser et al. [3] formulated an analytical expression that predicts the pressure distribution along the channels of the cell. By taking the following Equation 2.21 and providing the proper values, it is shown in Figure 2.2 that the pressure distribution along the center pass shows good agreement between the analytical solution and the numerical results. The data in Figure 2.1 have been normalized by the length (L) of a single pass and by the maximum pressure along the pass (P_{max}). The

agreement between these results provides further evidence that the model is capable of predicting physically realistic results.

$$P(z) = \frac{\Delta P_{cell}}{2N_c}\left(\frac{\sinh\left(m\left(\frac{z}{CL}-\frac{1}{2}\right)\right)}{\sinh\left(\frac{1}{2}\right)}+1\right) \tag{2.21}$$

In this equation, ΔP is the pressure difference along the center pass in the cell, N_c is the number of passes in the cell, CL is the length of a single pass, and m is a dimensionless quantity defined as $m^2 = 4\frac{L^2}{A_c}\frac{h_{GDL}}{\text{LW}}\frac{K_{ip}}{K_{chan}}$. In this expression, A_c is the product of the channel width and channel height, K_{ip} is the in-plane permeability of the GDL, and K_{chan} is the permeability of the channel. The channel permeability is approximated as a function of the the height to width ratio of the channel according to Feser et al. [3].

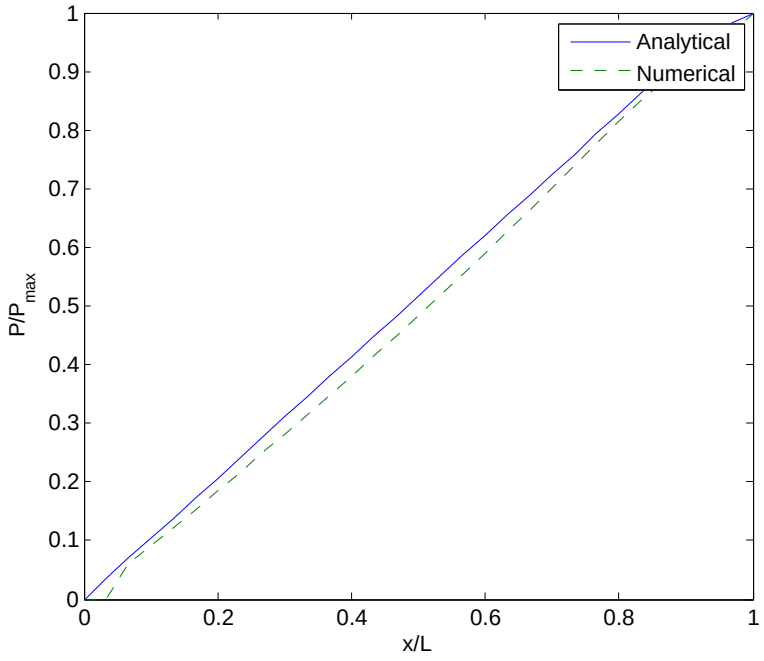

Figure 2.2: Comparison of numerical and analytical PEMFC pressure distribution along center pass.

2.6.3 Verification and Validation Summary

As a final check for physically realistic results, it is important to perform a global balance of charge. This check is done by comparing the consumed oxygen on the cathode to the charge produced by the cell.

Satisfactory results have been obtained to show that the PEMFC model used in this research is capable of producing physically realistic results. The only inputs needed by the gmesh script are the previously described dimensions to fully describe a single-serpentine channel configuration. The script is versatile enough to construct models with varied parameters and evaluate their respective performance. It is important to note that while the model is capable of modeling the polarization curve in Figure 2.1, this study will henceforth be focusing on a specific point on the curve. The reason is two-fold: first, the length of each run is significantly reduced if only one point on the curve is simulated, and second, comparison across different simulations is simplified. The selected point for comparison of the various flow channel geometries is the operating voltage of 0.6 V. This voltage was chosen so that the cell would be operating in the mass transport region of the polarization curve. The design of the channels has a direct impact on the mass transport losses. Therefore, it is important to make sure that the model is sensitive to performance changes in this region of the curve.

2.7 Chapter Summary

This chapter has provided the full description of a highly accurate PEMFC numerical model. For the purposes of this project, it was beyond the scope to formulate and numerically implement a PEMFC model. Currently available models are capable of performing this desired task. Therefore, the FLUENT PEMFC Add-on Module was selected to perform the modeling part of this thesis. The model's assumptions as well as the governing equations were provided in detail. The model was validated by comparison with both analytical and experimental results. All

required material properties and boundary conditions were summarized and will be used throughout the rest of this thesis unless otherwise noted. The next chapter will focus on the integration of this model into the GA optimization method.

Chapter 3

OPTIMIZATION METHODOLOGY AND AUTOMATION

3.1 Genetic Algorithm Overview

Within the subject of Evolutionary Computing there is an optimization method known as the Genetic Algorithm (GA), originally developed by Holland according to Sivanandam and Deepa [12]. The GA is an optimization technique that employs the fundamental principles that drive natural evolution. The strength of the GA is its ability to efficiently locate optima within relatively large search spaces. In order for a GA to be implemented, a system must first be reduced to the basic parameters that are needed to describe it. Once these parameters are identified, the GA can go to work on determining the optimum values for these parameters. This chapter will focus on an explanation of the theory behind the GA and its integration into the PEMFC optimization methodology of this research project. The GA used in this study is the commercially available Genetic Algorithm and Direct Search Toolbox provided in MatLab.

3.2 Genetic Algorithm Theory

The description of the GA in this research parallels the conventional terms used when discussing genetics. An individual is defined by the genes that make up its chromosome. In this project, the chromosome is responsible for describing a unique PEMFC individual (IND). Each individual has a specific number of genes. For a three parameter optimization, there are three genes, one for each of the parameters.

The genes in this research include the channel width, land width, and channel length; each parameter is bounded with a selected upper and lower bound. The relevant schematic diagrams are discussed later int Chapter 4 and Chapter 5. These bounds set the range of allowable values that can be assigned to that parameter. The bounds are set based on known guidelines to be followed for general fuel cell design. It would not be efficient to include ranges of values that are known a priori to result in poor performance.

The performance of an individual is determined by applying an appropriately formulated fitness function in the GA. The fitness function is responsible for minimizing or maximizing a quantity of interest. In the case of the PEMFC, the fitness function is defined as the net power density. Once the GA has been given a set of values that defines the search space, it is possible to begin the optimization process. The GA includes the crossover process within its set of functions. The crossover process takes place between successive generations. The current generation is created by examining the genes of the individuals in the previous generation. The genes of the best individuals are crossed with those of other individuals which showed good performance. The new individuals are comprised of different combinations of the genes in the initial generation.

The purpose of crossover is to create combinations of genes that outperform individuals of the previous generation. Herein lies the problem; until this point, the best individual possible is generated by selecting the best combination of previously-generated values for each of the parameters. There is the possibility that not enough different parameter values were available in the previous generation and therefore, a possibly better individual is incapable of being created. The GA resolves this issue by employing a powerful technique which is borrowed from evolutionary biology: random mutations are incorporated into the creation of individuals in new generations. Random mutations help to dislodge a solution that may have settled on a

local optimum and propel it towards the desired global optimum. The mutation rate is set so as to not create completely random individuals, but rather to include a limited amount of randomness between successive generations. While the method does not guarantee that the global optimum will always be found, it is generally accepted that the final solution will be close to the global optimum as long as successive generations are incapable of producing better individuals. Not finding the exact global optimum is a trade off for saving computational time and power.

The GA finds the optimum solution with far fewer simulations than an exhaustive brute force parametric study which evaluates the performance of each of a vast array of possible individuals. Hence, the GA search method saves both time and resources while determining the parameter values that predict the best individual. The MatLab Genetic Algorithm and Direct Search Toolbox is capable of executing such a scheme along with many other options that are necessary to control a GA optimization. This toolbox is fully integrated with the automated process that optimizes a PEMFC in this research. The following sections will outline the options that guide the GA and the integration of each of the software tools that are required to automate the optimization and solution processes.

3.2.1 MATLAB GA Toolbox set parameters

Table 3.1 summarizes the GA parameters that are used throughout this study. The elite count is the number of individuals that go from one generation to the next unchanged. These elite individuals are the best performers of a given generation and are used to crossover and create the rest of the population in a given generation. The crossover rate can range from 0-1 and represents the fraction of the next generation that is comprised of crossover offspring. The remaining offspring are comprised of mutated individuals. The stall time limit is set to infinity in order to eliminate the possibility of terminating the PEMFC model before completing a simulation. The tolerance values are set to terminate the GA process if successive generations

do not create new individuals whose performance improvement exceeds tolerance value. This setting would suggest that the optimum was reached and the individuals converged to the best solution within the search space. The fitness scaling function puts the individuals of a given population in rank order instead of ranking them by their fitness values. The best individual is ranked number 1, and so on. The ranking of individuals removes the effects of the spread between raw fitness scores.

Table 3.1: Conservation of Energy Source Terms

GA Setting	Chosen Setting
Elite Count	2
Crossover Fraction	0.8
Stall Time Limit	Infinite
TolFun	1e-6
TolCon	1e-6
Creation Function	Uniform
Fitness Scaling Function	Rank
Selection Function	Stochastic Uniform

3.3 Communication Script

Now that the the GA settings have been fully defined and the optimization process has been described, the process of evaluating an individual's fitness needs to be discussed. This study represents the first instance in which GA optimization has been coupled with an automated scheme capable of constructing unique PEMFC models and evaluating their performance. Although previous studies have investigated PEMFC performance parametrically, none have been aimed at finding the optimal channel characteristics of a customizable area. The following script is capable of automatically generating a solid model for a fuel cell of a chosen design and size. The channel geometry that produces optimum performance for a cell of a certain size need not be the same as that for a larger cell. The benefit of our script is the scalability of the process; an optimum geometry can be found for a cell of any

size, automatically and efficiently. This research will identify the optimum values for (1) a three-parameter single serpentine configuration, and (2) for a five-parameter double-serpentine configuration.

Several scripts were written to control and integrate all of the software packages necessary to run the optimization. Figure 3.1 summarizes the process herein. The user sets the number of parameters to be optimized as well as the upper and lower bounds for each parameter. Once the previously discussed GA options are set and the search space is chosen, the GA optimization is ready to begin.

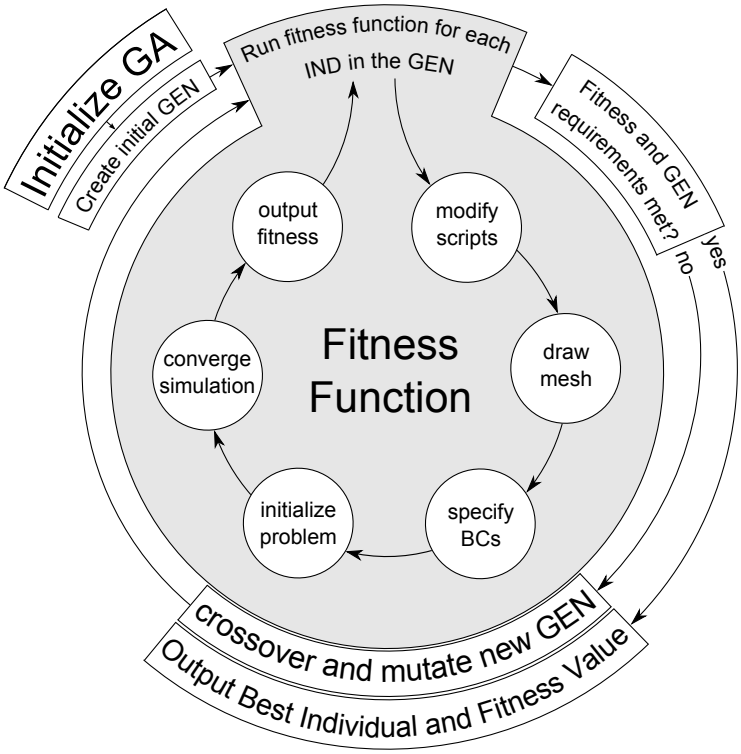

Figure 3.1: GA Flow Chart

At this point, the GA Toolbox creates random sets of parameter values for each of the individuals in the initial population. This initial population is referred to as Generation (GEN) Zero. The GA evaluates the fitness of each individual by

calling the Fitness Function (FF). The fitness function is the second script that was created to control the optimization. This script is responsible for the integration of all of the software packages and extracts the appropriate data to calculate the fitness of an individual. The script calculates the fitness of each individual of the generation, one at a time. The fitness function receives as input the values for each of the genes that describe an individual. Each of the values is written to a GAMBIT journal file. The GAMBIT journal file, Gmesh, is the third script in this process. It is designed to draw a solid model according to the input parameter values. It then populates the model with an appropriately scaled mesh and applies the boundary condition types and zone types to the PEMFC domain. Once the model is fully constructed, the mesh is written to file.

The FF script next calls the FLUENT journal script, Fjou. The Fjou script is responsible for loading the PEMFC module, applying all material types to each of the zones, applying values to each of the required boundary conditions, initializing the solver, setting convergence criteria, converging the solution, and saving the appropriate solution values to a file. The Gmesh script takes the raw data from the Fjou output files and uses it to calculate the fitness of each individual. This final value is returned to FF and sent back to the GA control process. This process is repeated for each of the individuals that the GA requests for each generation.

Some specific strengths of the scripts are as follows:

- The Gmesh script calculates the number of passes that are necessary to fill a given area. eg. single-, double-serpentine
- The Fjou script can handle any Gmesh script with appropriately named zones.
- The operating conditions are easy to access if alterations are desired.

Once the specified number of generations is reached, or the convergence criteria for successive generations are met, the GA is completed. The GA then outputs

the best individual of the entire population and the parameter values that describe it. This individual represents an optimum configuration within the search space and the process is complete. The individual can then be compared to other individuals in the population to determine the characteristics that strongly influenced performance. The information that is gathered from the population as a whole can be used to design and initialize future GA studies in order to decrease convergence time and increase performance.

3.4 Summary

This chapter contains a definition of the parameters that are required to initialize a GA and presents a description of the relevant terminology. The optimization process has been described in detail including the integration of various stand-alone software packages. These packages include GAMBIT for the solid modeling and meshing, FLUENT for the PEMFC solver, and MATLAB for the GA control script. The integration of all necessary software packages has allowed for an automated and efficient optimization process. The remainder of this thesis focuses on the application of this unique optimization scheme to the design of channel configurations for two types of PEMFC bipolar plate designs. Chapter 4 focuses on a three-parameter single-serpentine channel configuration and Chapter 5 extends the optimization to a five-parameter double-serpentine configuration.

Chapter 4

SINGLE-SERPENTINE CHANNEL OPTIMIZATION

4.1 Introduction

The focus of this chapter is on the application of the GA-based optimization method described in Chapter 3 to a search space associated with the single-serpentine channel configuration. The optimization employs the PEMFC model described in Chapter 2 as a tool to calculate the quantities required to evaluate an individual's fitness. The population that is generated by the GA provides data for each individual. The relative performance of selected individuals identified by the optimization process is discussed here in order to understand how the design parameters influence the dominant physical mechanisms of the optimal individual chosen by the GA. The chief deliverable of this chapter is the set of three parameters that optimize a given PEMFC nominal area for maximum net power output.

4.2 Problem Definition

The GA optimization scheme for this study uses a population of eight individuals for each generation. There is a limit of 12 new generations above the initially randomized population that is generated. These limits are summarized in Table 3.1 and require each new generation to select two elite individuals from the previous generation. These two elite individuals are used to create four crossover offspring. The remaining two individuals of each generation are created by the mutation function. The generations stop either when the individuals of successive generations do

not improve by an amount exceeding the set tolerance limits, or when the maximum number of generations is reached. The entire population consists of 104 individuals, however, since the elite individuals pass unchanged between generations, the number of unique individuals that need to be evaluated is equal to 80. The fitness function script prevents the reevaluation of individuals by checking a continually updated database for repeat individuals during the optimization.

The search space for the design of this PEMFC is defined by prescribing ranges of values for the three independent parameters: channel length (CL), channel width (CW), and land width (LW). The channel length is defined as the length of a single pass of the serpentine channel, as opposed to the overall length of the entire serpentine channel from inlet to outlet. The three parameters are depicted schematically in Figure 4.1.

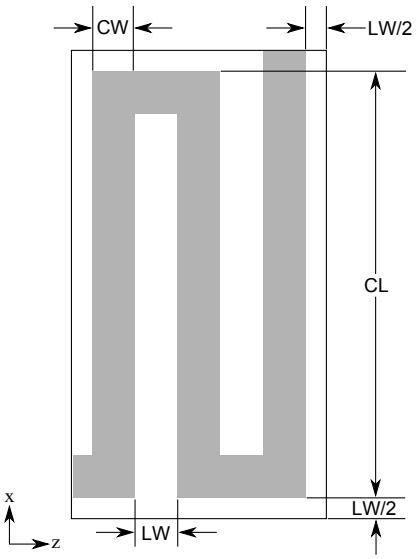

Figure 4.1: Schematic of the three-parameter single-serpentine configuration.

The active area of the fuel cell extends beyond the outer edges of the channel in the xz-plane by an amount equal to one-half of the specified land width as shown

in Figure 4.1. The nominal area (A) of the cell is set at a target of 16 cm^2. The range of values for each of the parameters is summarized in Table 4.1. The channel height is set to a constant value of 1.0 mm. The Gmesh script uses the three parameter values to calculate the number of passes that are required to fill the nominal area with the given channel width, land width, and channel length. The number of passes is rounded to the nearest odd integer in order to create a cell with the desired channel configuration in which the inlet and outlet ports are on opposite sides of the cell. This condition maintains the same inlet and outlet configuration for all individuals. The PEMFC is designed with counter-current flow channels such that the inlet and outlet ports of the anode are reversed for the cathode. The anode and cathode channels overlay exactly on top of each other when projected on to the xz-plane.

Table 4.1: Three Parameter Search Space

Parameter	Lower Limit	Upper Limit
Channel Length	4.0 cm	14 cm
Channel Width	0.5 mm	1.5 mm
Land Width	1.0 mm	3.5 mm

The power density of a cell at a fixed voltage is the product of its current density, i, and its voltage, V. This quantity is the gross power density under the chosen operating conditions. However, in practice, a fuel cell system incorporates the balance-of-plant consisting of several components whose input power is drawn from the fuel cell itself. The cumulative power requirement of all the associated components represents a quantity known the cell's parasitic power loss. Of particular relevance to this study, the power requirement of the motor and compressor assembly for the air supply system is largely influenced by the channel geometry. Therefore, it is appropriate to include the parasitic loss associated with driving air through the cathode channels as a factor in the fitness function. Each channel configuration within the search space imposes a power requirement that is proportional to the total pressure drop from inlet to outlet and the mass flow rate through the channel. A

small channel cross-sectional area and long overall channel length results in a much higher pressure drop than a channel with a large cross-sectional area and short overall channel length. Equation 4.1 found in Larminie and Dicks [8] approximates the parasitic power requirement of a cell.

$$P_{par} = c_p \frac{T_{amb}}{\eta} \left(\left(\frac{p_{in}}{p_{amb}} \right)^{\frac{\gamma-1}{\gamma}} - 1 \right) \dot{m} \tag{4.1}$$

In this equation, the motor and compressor efficiency is assumed to be $\eta = 0.7$ and the heat capacity ratio of air is set as $\gamma = 1.4$. T_{amb} is the ambient temperature, p_{amb} is the ambient pressure, and p_{in} is the pressure at the inlet of the PEMFC. The inlet pressure is calculated by FLUENT and is part of the data output of the Fjou script. The mass flow rate of air is calculated using Equation 4.2 which is also found in Larminie and Dicks [10].

$$\dot{m}_{air} = 3.57 \times 10^{-7} \cdot \lambda i A \tag{4.2}$$

Here, i the current density of the cell, A is the nominal area of the cell, and the stoichiometry is set to $\lambda = 2$. Similarly, the hydrogen flow rate is calculated using Equation 4.3.

$$\dot{m}_{H_2} = 1.05 \times 10^{-8} \cdot \lambda i A \tag{4.3}$$

Both reactant gas mass flow rates correspond to the stoichiometry of $\lambda = 2$ at 1 A/cm^2, which is a common condition used when evaluating PEMFC performance. With all of the required quantities defined, the net power is now calculated in Equation 4.4. The parasitic power loss does not include any loss due to the supply of hydrogen to the anode side. The hydrogen is supplied from a pressurized vessel, and therefore requires no external compression.

$$P_{net} = P_{cell} - P_{par} \tag{4.4}$$

The power of the cell, P_{cell}, is calculated by the PEMFC module and is the product of the cell's current density, nominal area, and voltage. The fitness function is now defined in Equation 4.5 as the desired quantity of net power per unit area.

$$FF = -\frac{P_{net}}{A} \tag{4.5}$$

The negative sign is included in the fitness function because the MatLab GA technique works only by minimizing a quantity. Since the magnitude of the quantity of interest needs to be maximized, the largest negative value then becomes the minimum value, and the power density is therefore maximized. Once the simulation is complete, the absolute value of the fitness function represents the net power density of each individual. The remainder of this chapter focuses on the analysis of the data collected during the GA optimization process.

4.3 Optimization Output

As the GA progresses through each generation, a useful way to monitor the GA's performance and convergence is to plot of the average fitness of a generation and the fitness of the best individual of that generation. This convergence history is presented in Figure 4.2.

This GA optimization strategy resulted in 106 uniquely created individuals. These individuals covered a wide range of parameter values within the limits set in the GA. The performance corresponds to the fitness function defined in Equation 4.5. Because the fitness function is the net power density as opposed to the gross power density, the individuals are ranked more accurately on how they would perform in a real world setting. Figure 4.2 indicates that the fitness function rapidly improves within the first six generations and then eventually converges to the final value. Evidently, the GA is an effective method for this type of optimization study.

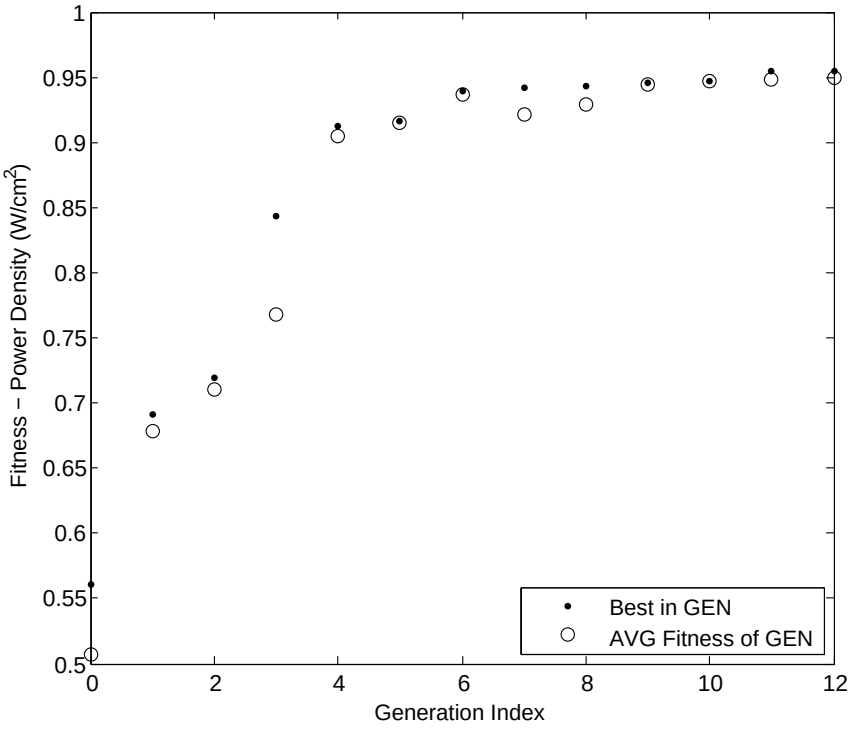

Figure 4.2: Convergence of GA population toward the "best" individual.

4.4 Comparison of Best and Worst individuals

The focus of this section is on the comparison between the best and worst individuals in the population whose parameter and output values are summarized in Table 4.2. This comparison aids in the explanation of the reasons why two individuals within a reasonable search space produce very different performance values. The net power density of the worst individual is 50.7% lower than the best individual.

The investigation of these individuals begins by examining the current density distributions on the surface of the cathode catalyst layer of each individual. Figure 4.3 shows the current density magnitude on the interface of the GDL and

Table 4.2: Three-Parameter Study: Best and Worst Individuals

Quantity or Parameter	Best	Worst
Channel Length	4.64 cm	4.00 cm
Channel Width	0.762 mm	1.11 mm
Land Width	0.934 mm	3.50 mm
Net Power Density	0.954 W/m^2	0.474 W/m^2

CL on the cathode side of the cell where the oxygen reduction reaction takes place. Areas of relatively high current density indicate that oxygen is reaching those sites. The figure shows that the worst individual is unable to utilize the catalyst sites under the land regions of the cell. The best individual makes better use of the areas under the land for producing current in the cell. Another observation is that the inlet and outlet regions do not produce much current density in either of the individuals. This happens because of the counter-current flow configuration used in the cell. By the time the reactant flow reaches the outlet, reactant depletion lowers its partial pressure, which starves the region of either oxygen or hydrogen and therefore limits the reaction. In the worst individual, most of the land is unused. The majority of the current is produced under the channel and is collected by the ribs of the bipolar plate. The reason for the poor utilization of active area under the lands in the worst individual is the high land width of 3.5 mm. Reactant gas is unable to diffuse far under the land and results in mass transport loss leading to poor current density.

The next step is to investigate the oxygen consumption within the cell. When a PEMFC cathode is fed with air instead of pure oxygen, the reaction is more likely to be limited by the oxygen content of the air between the inlet and the outlet of the cell. To understand why a given cell is performing well, it is important to examine the local consumption of oxygen and correlate it to the overall performance of the cell. Figure 4.4 compares the best and worst individuals in terms of the oxygen concentration in the cathode channel midplane.

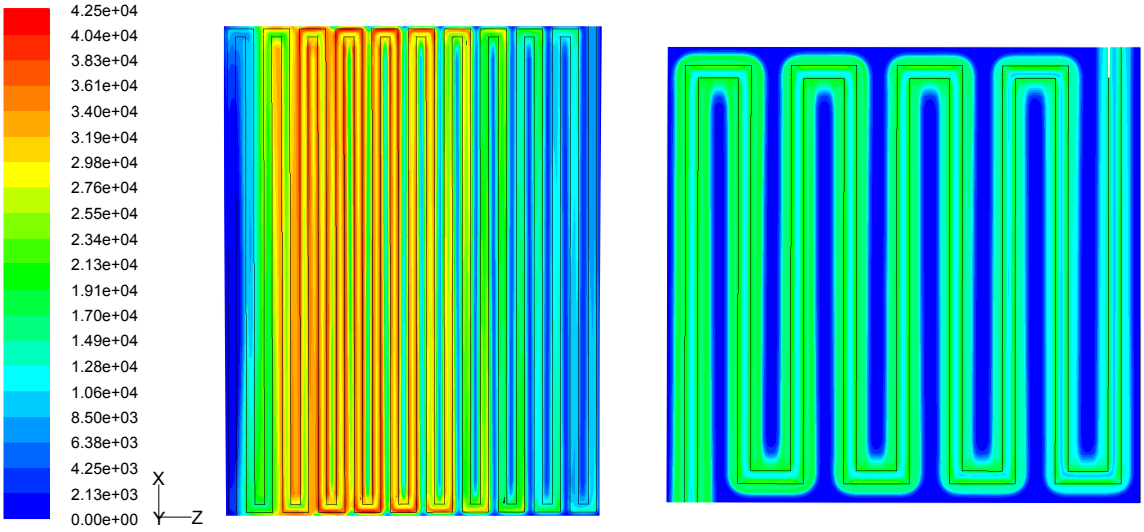

Figure 4.3: Best and worst individuals' contour plots of current density (A/m^2) at the cathode GDL and CL interface.

Figure 4.4 shows that the oxygen is almost completely depleted by the time the flow reaches the outlet of the channel for the best individual. This observation confirms that oxygen consumption is high for the best individual resulting is high overall current density. On the other hand, the worst individual's outlet concentration is still quite high, about half of the inlet concentration. The main reason for this is the reduced oxygen consumption due to the channel's inability to deliver reactants to the catalyst layer underneath the wide land regions. The wide land width of 3.5 mm increases the resistance to convective bypass between adjacent channels. Convective bypass, as defined in Chapter 2, is the primary mechanism that delivers reactant gases to the catalyst layer. The channel length for this cell does not allow a large enough pressure drop to build in each return pass to drive adequate convective bypass under the wide lands for the worst case.

Convective bypass underneath the lands is proportional to the pressure difference between two adjacent channels in a cell. The largest pressure gradient is

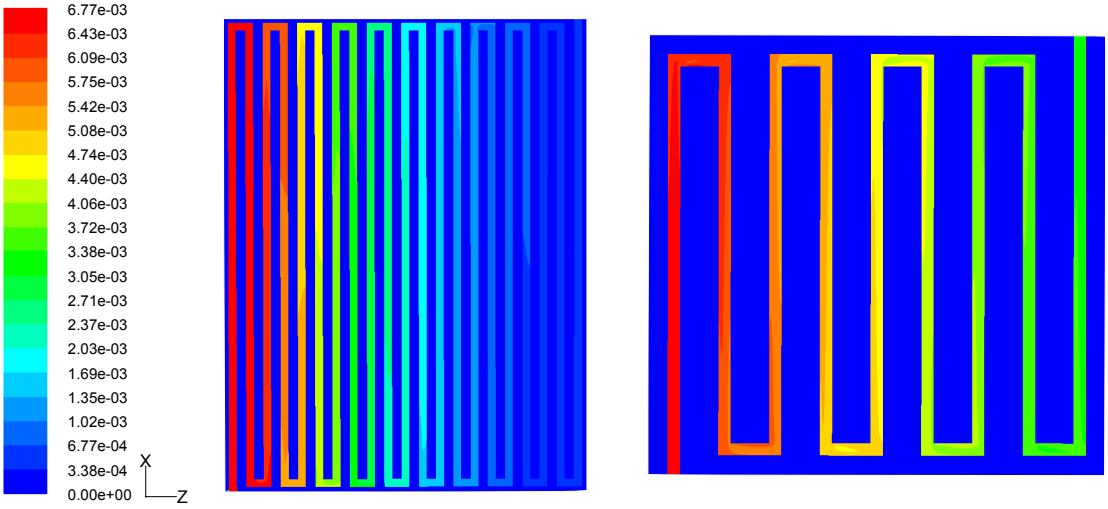

Figure 4.4: Best and worst individuals' contour plots of oxygen concentration (kmol/m^3) along the cathode channel.

located at the roots of adjacent channels, at the end that is opposite to where the channel makes a U-turn. This large pressure difference drives the air and hydrogen into the GDL and the CL under the lands, as well as driving out product water from under the lands. The reaction however, can proceed only if there is an adequate proton flux through the membrane from the anode side to complete the reaction on the cathode side. If the hydrogen concentration is depleted such as near the hydrogen outlet, then not enough hydrogen is forced into the GDL and the reaction and current production are weak. These regions are known as dead zones in a PEMFC and should be minimized as much as possible. Figure 4.5 shows that there is still a significant concentration of hydrogen at the outlet of the worst performer, while the hydrogen is almost completely depleted by the time the flow reaches the outlet of the best individual.

The contour plot of oxygen concentration in three layers (top, middle and bottom) of the cathode GDL in Figure 4.6 shows that there is oxygen under both the channel and the land for the best performer. This figure also shows that oxygen

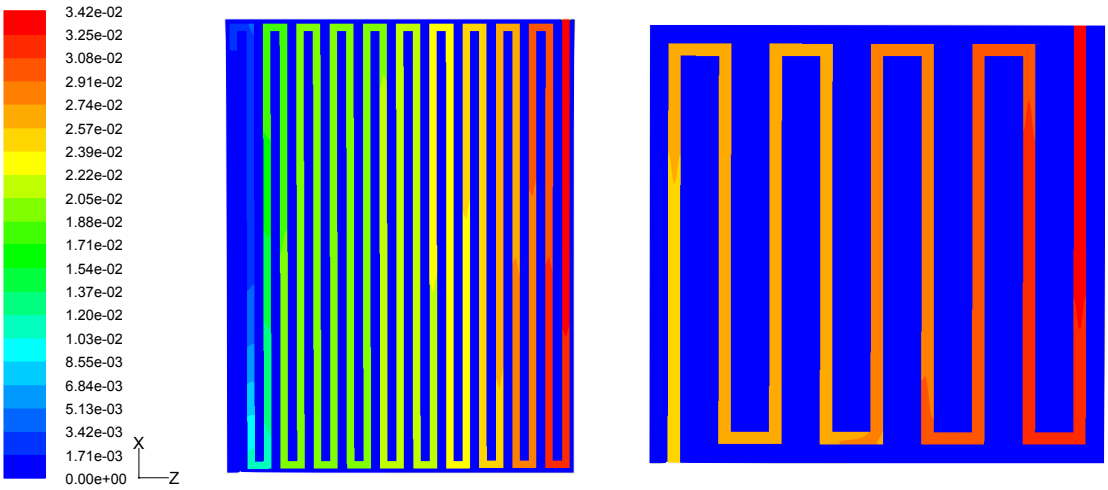

Figure 4.5: Best and worst individuals' contour plots of hydrogen concentration (kmol/m^3) along the anode channel.

is driven towards the catalyst layer by the concentration gradient of oxygen in the y-direction. Oxygen flows through the thickness of the GDL parallel to the y-axis and is consumed directly below the channels. In addition, oxygen is also being delivered to the catalyst under the land areas.

The velocity vectors in Figure 4.7 show that air is driven by convection under the ribs of adjacent passes for the best performer. Therefore, oxygen is delivered effectively to the catalyst layer even below the land areas. This is a desirable result because all of the catalyst area is able to participate in the reaction. In contrast, the velocities under the cathode lands in the case of the worst individual are not very high, implying that diffusion is the dominant transport mechanism for oxygen. Diffusion is not as effective in transporting reactant gas under the lands, and therefore, although the oxygen concentration is high under the channels for the worst individual, it experiences low oxygen concentration under the lands. Contrary to this result, the best performer shows evidence of both diffusive and convective transport.

The absolute pressure distribution within the channels and the GDL provides

insight into the velocity distributions found in the GDL. Figure 4.8 presents the pressure distribution along the midplane of the GDL on the cathode side of the cell for the best and worst performers. The pressure gradients are highest in the vicinity of the channel roots at each pass. In the best individual, the pressure gradient is very effective at driving convective bypass under the land areas of the cell. The worst individual again suffers because the pressure gradient is insufficient to drive convective bypass across the wide lands. The overall pressure difference across the cell is small owing to the small number of passes, and hence the small total channel length. The pressure distribution is an important indicator of the cell's performance. The pressure distribution is mainly determined by the configuration of the gas flow channels. This result further validates the usefulness of this study to determine the optimal channel configurations for a specified cell area.

4.5 Comparison to neighbors

The data presented thus far have shown that, of a given set of individuals, there is clearly one that performs the best. The preceding discussion has also helped to explain the mechanisms that contribute to its good performance. Keeping in mind that the set of individuals that was actually evaluated is just a small subset of all the possible individuals the search space encompasses, it is necessary to provide more evidence that the "best" individual is indeed the best of all possible individuals. The only way to prove this conclusively is to perform an exhaustive study of all of the combinations of the parameter values. This type of brute-force study is prohibitively expensive, and the GA technique was chosen in the first place to precisely avoid such an exercise. A simpler approach is to examine the neighboring individuals with parameter values adjacent to those of the best individual and thereby confirm that the best individual is superior to its neighbors. Ideally, the GA should have ignored such inferior individuals and converged to the best individual. Accordingly, a "bracketing" study was performed in which each parameter value was varied from the

optimum value while keeping the other parameter values fixed, and the performance of the new individuals was observed. Figure 4.9 shows the performance of the individuals neighboring the best performer. In this figure, data were only obtained for parameter values indicated by the data points; the lines connecting the data points are provided only for clarity.

The adjacent individuals, or neighbors, are created by scaling each parameter by $\pm 5\%$ and $\pm 10\%$. This results in 12 new individuals for whom the corresponding fitness values were evaluated. Figure 4.9 shows that while all of the new individuals performed well, none were able to out-perform the best individual. This plot has two interesting characteristics. First, the GA did indeed correctly identify the best individual within this parametric "bracketing" study. Second, the best performer occupies the peak of a relatively flat performance region. The neighbors surrounding the best individual show a performance drop of no more than 2% of the optimal configuration. This observation suggests that while performing the study on this size of a PEMFC, it is important to isolate channel parameters that are near the optimum value, and that being very close to the best performer is also a very good result.

Upon inspecting Figure 4.10, it becomes obvious why the fitness function was chosen to include the parasitic power losses associated with driving the gas flow through the cell. The parasitic power loss does not vary monotonically with the gross power output of the cell; i.e., a ranked order of best performers by net power would not be identical to a similar list ranked by gross power. This is because for a given cell area, the channel configuration can take on various channel geometries. The narrower the channel cross-sectional area and the longer the overall channel length, the higher the pumping requirements of the cell. Therefore, it is necessary to account for the parasitic power losses to accurately gauge PEMFC performance.

4.6 Summary

This chapter has focused on the optimization of a three-parameter single-serpentine channel configuration. The best possible individual was automatically determined by the GA and reasons for its superior performance were discussed. The GA was proven to effectively search a space for the best individual by means of a bracketing study which demonstrated that the best performer is indeed superior to all its neighbors in parameter space. The next chapter will focus on applying the same optimization method to a double-serpentine, five-parameter channel design. This design will be applied to the same fuel cell active area as this study, and the relative performance of the best individuals between the three- and five-parameter studies will be discussed.

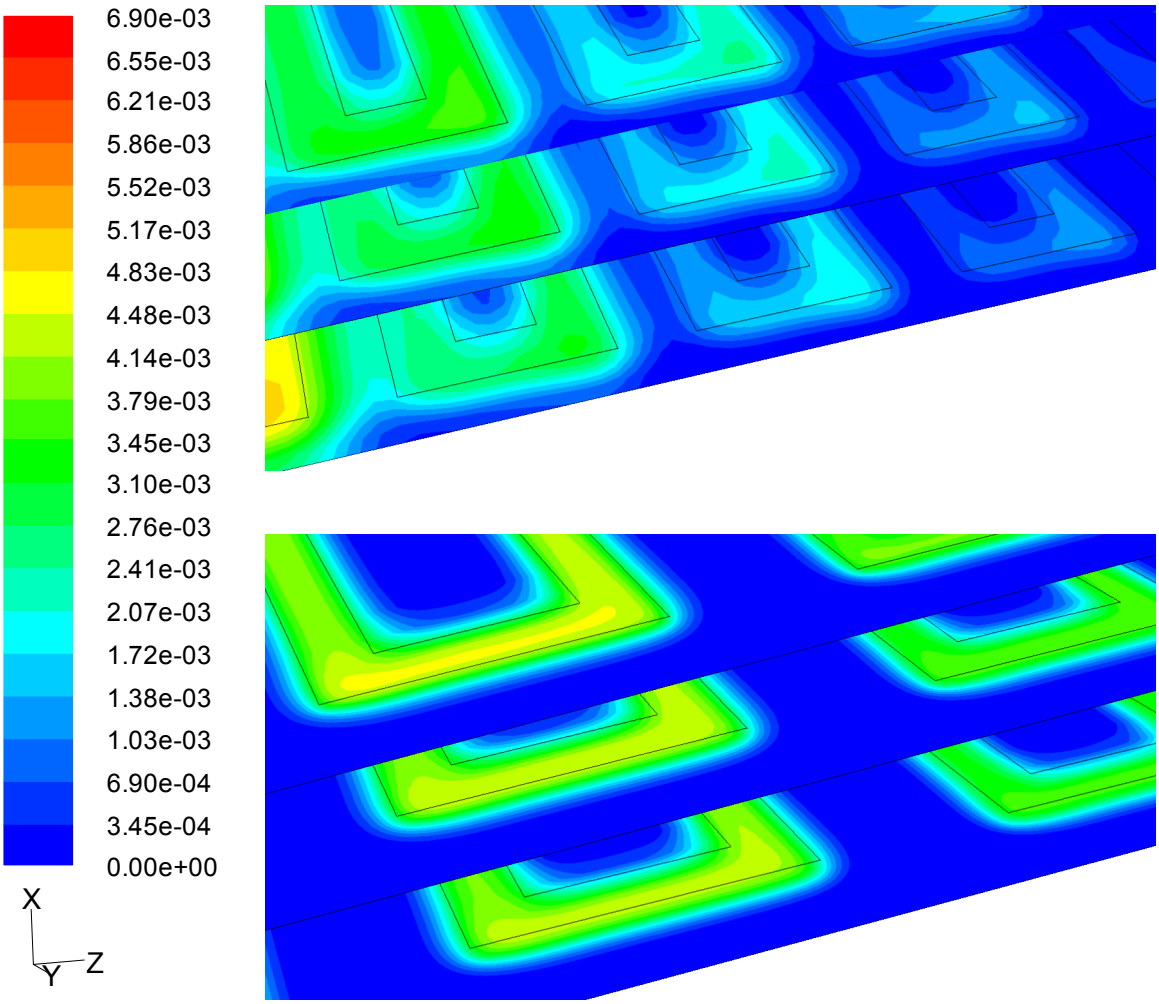

Figure 4.6: Oxygen concentration (kmol/m^3) at the top, middle, and bottom of the cathode GDL for the best (left) and worst (right) performers.

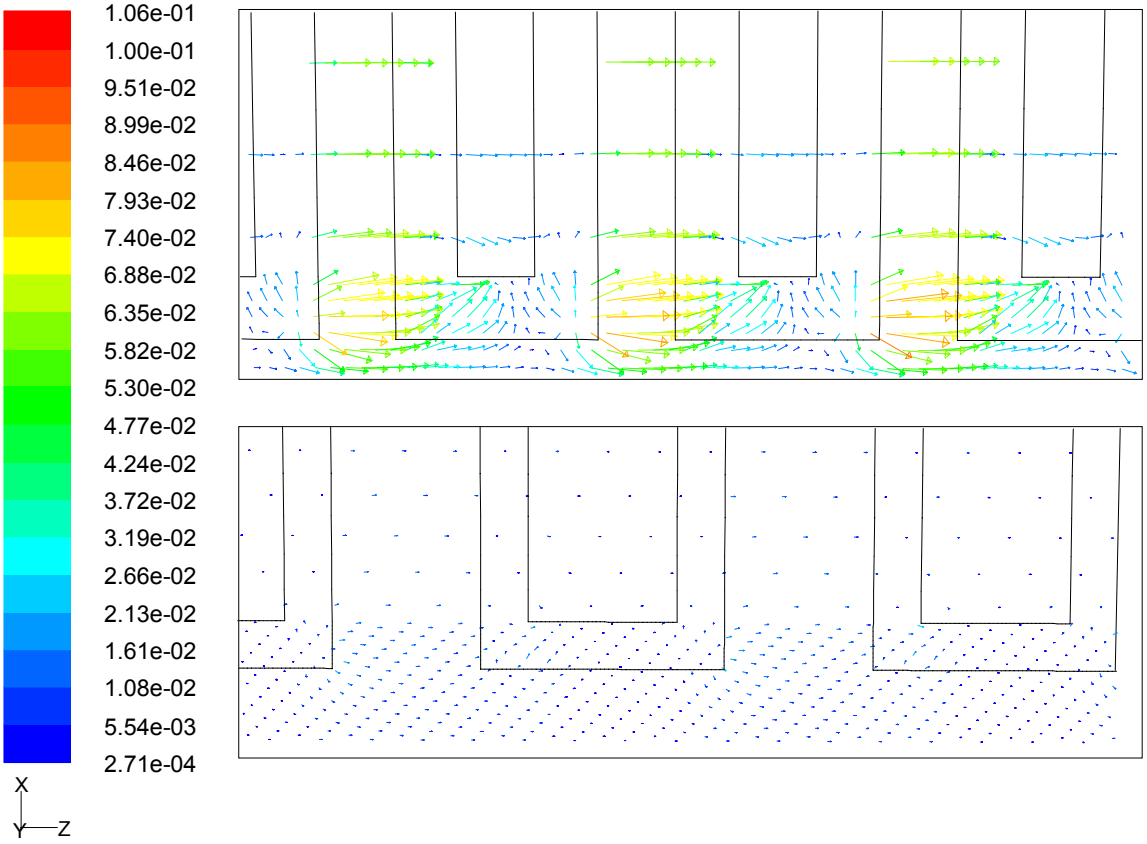

Figure 4.7: Velocity vectors (m/s) in best (top) and worst (bottom) individuals of the cathode GDL. Velocities correspond to the midplane of the GDL

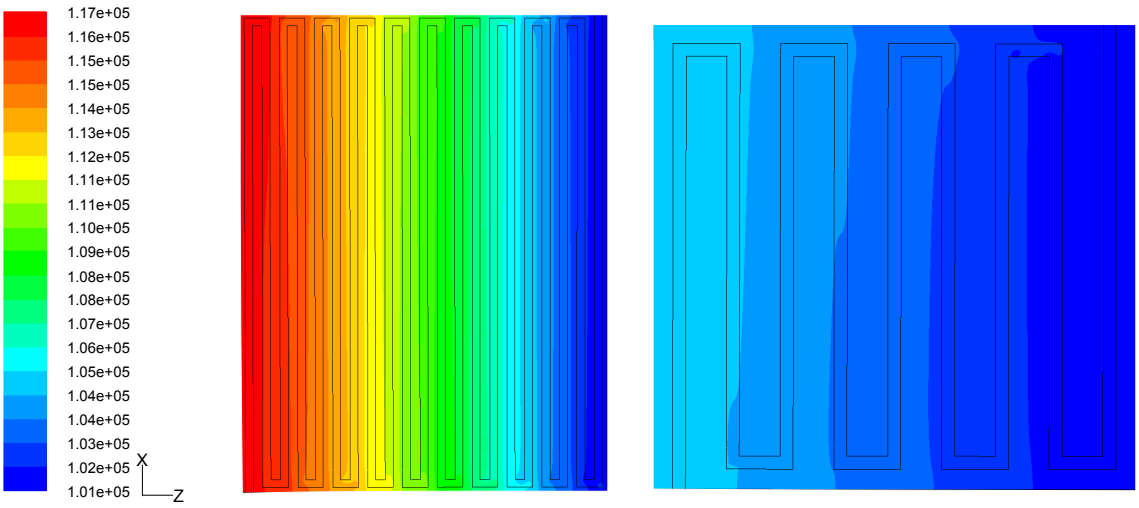

Figure 4.8: Absolute pressure (Pa) in the cathode GDL mid-plane for the best (left) and worst (right) performers.

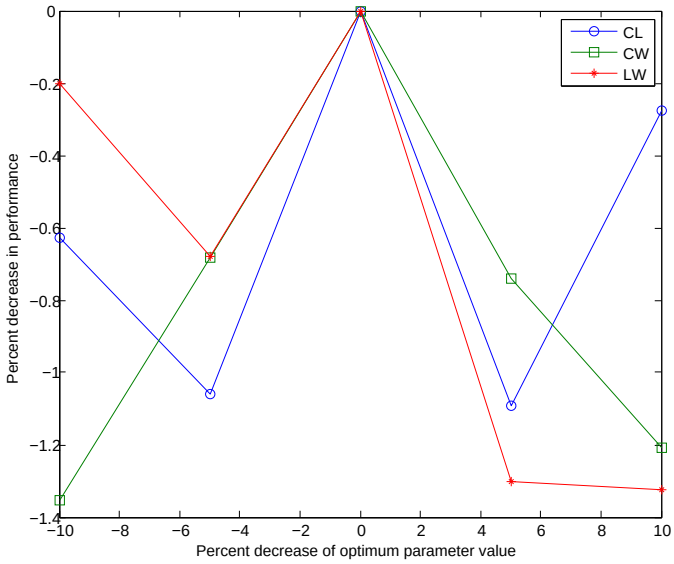

Figure 4.9: Result of a bracketing study that compares the fitness of neighbors to the fitness of the best individual.

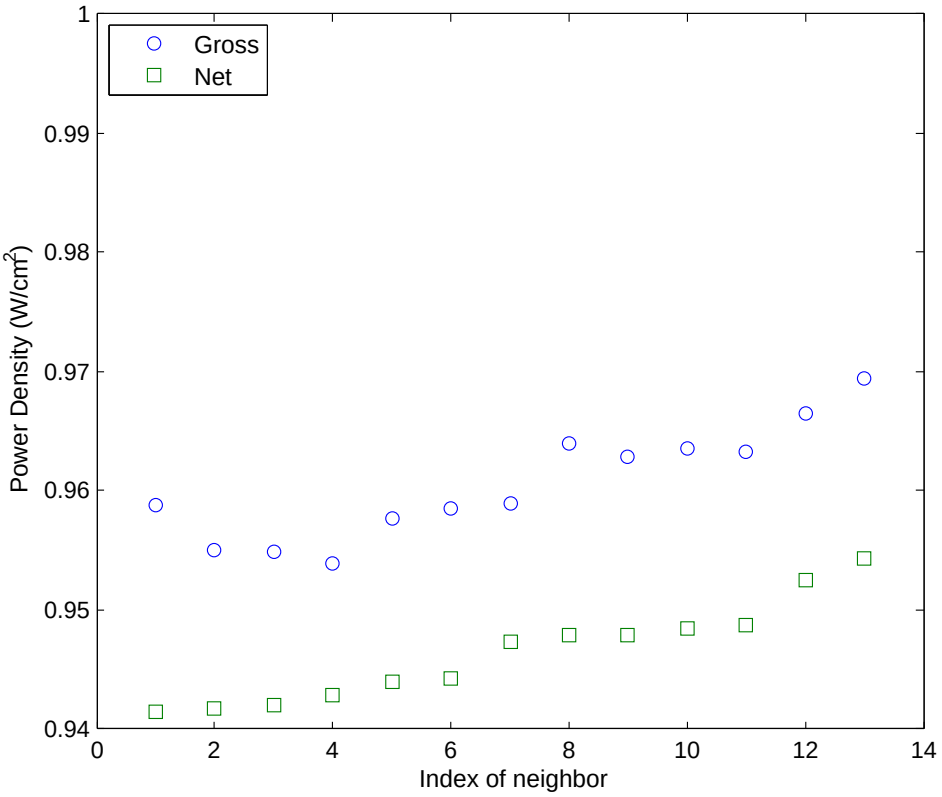

Figure 4.10: Gross and net power density comparison of neighbors to best individual.

Chapter 5

DOUBLE-SERPENTINE CHANNEL OPTIMIZATION

5.1 Introduction

The focus of this chapter is on the application of the GA-based optimization method to the search space of a double-serpentine channel configuration that includes five independent geometric design parameters. Each of these parameters is controlled by the GA script which was outlined in Chapter 3. The search space of this study is significantly larger than that of the three-parameter study conducted in Chapter 4. The effectiveness of the GA is revealed in that the number of individuals that need to be tested does not increase linearly with the number of possible individuals in a search space. For example, if each parameter was assigned five possible values, there would be $5^3 = 125$ single-serpentine individuals, and $5^5 = 3125$ double-serpentine individuals to be evaluated by a brute force parametric study. However, by applying GA, the total number of individuals only increased from 104 to 130. This comparison reveals the effectiveness and power of the GA when used in conjunction with the automatic domain, meshing, and modeling tool developed for this research project. The chief deliverables of this chapter are (1) the set of five parameter values that optimize the double-serpentine channel geometry within a specified nominal area of a PEMFC for maximum net power output, and (2) a comparison of the optimal individuals of the single- and double-serpentine channel designs for a 16 cm^2 PEMFC.

5.2 Problem Definition

The optimization for this problem uses the same GA options that are outlined in Section 3 of Chapter 3 and uses the same boundary conditions, geometrical constraints, and fitness function as the three-parameter study of Chapter 4, aside from the exceptions that are discussed in this section. The number of individuals that comprises each generation is increased to 10 with a limit of 15 generations beyond the initial generation which uses randomly-assigned parameter values. The GA returned 130 unique individuals whose fitness functions were evaluated during the study. The same meshing strategy and convergence rules apply to the models created in this search space as outlined in Section 4 of Chapter 3.

The double-serpentine channel configuration studied in this chapter uses five independent parameters which include two channel widths, two land widths, and one channel length. The channel length of the double-serpentine channel configuration is defined as the total distance that the double channel requires to make one switchback. The Gmesh script discussed in Chapter 3 constructs a border for the PEMFC that surrounds the outer edges of the channel in the xz-plane with a width equal to half of the average of the two land widths of the associated individual. These parameters are depicted schematically in Figure 5.1. The Gmesh script uses these five parameters to calculate the number of channel passes that are needed to fill the required nominal area of the cell.

The Gmesh script for this model is a modified version of the Gmesh script used for optimization in Chapter 4. It includes the necessary changes for the new channel configuration described by the above parameters as well as modifications to the inlets and outlets. Our PEMFC model requires the specification of the mass flow rate supplied at the anode and cathode inlets. It is desirable to construct the channels in such a way that only one inlet and one outlet condition need to be specified for both the anode and the cathode. Accordingly, an inlet manifold is constructed

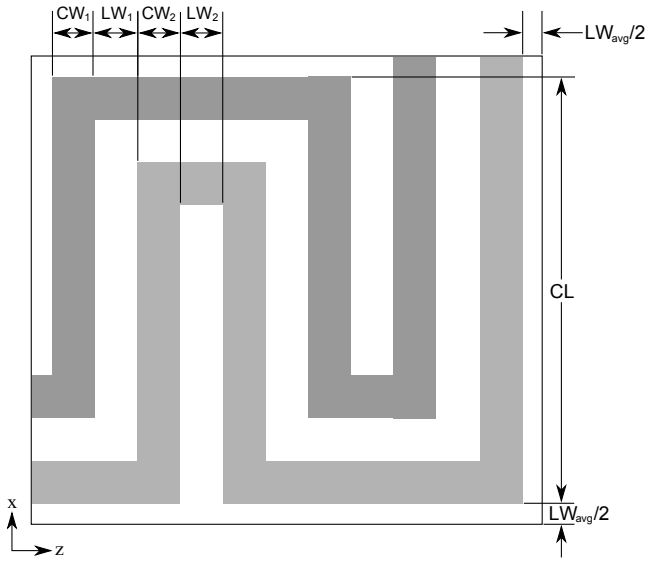

Figure 5.1: Schematic of the five-parameter (CL, CW_1, CW_2, LW_1, LW_2) double-serpentine configuration.

to connect the two inlet channels at both the anode and cathode. Figure 5.2 depicts the manifold that was included in the Gmesh script. The schematic shows an example of one inlet manifold and is representative of each inlet and outlet manifold of the cell. By connecting both channels of the double-serpentine configuration with the inlet and outlet manifolds, the geometry accurately describes the physical arrangement for reactant delivery to the cell.

The boundary conditions described in Chapter 4 remain the same for the double-serpentine study. The fitness function shown in Equation 4.5 also remain the same. The Fjou script that runs the FLUENT simulation remains unchanged because the model is defined by the same zones and boundary condition types. Table 5.1 summarizes the range of values within which each of the five parameters is allowed to vary. The limits define the extent of the search space in this optimization study. The channel height is set to 1 mm. Since the land width of 3.5 mm performed poorly during the three-parameter optimization in Chapter 4, the upper

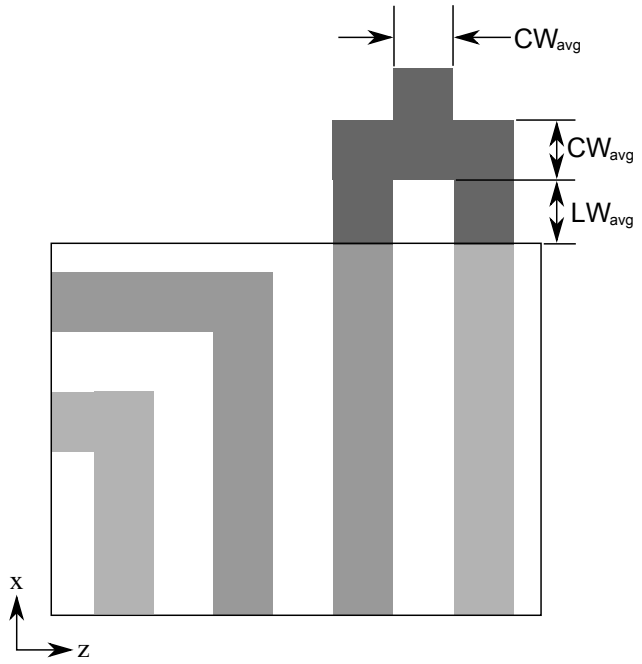

Figure 5.2: Schematic of the double-serpentine manifold.

limit of LW was reduced in this optimization study to 2.5 mm. The aim of this change was to exclude regions of the search space that would arguably return inferior individuals and instead concentrate on individuals with a higher probability of good performance.

Table 5.1: Double-Serpentine Search Space

Parameter	Lower Limit	Upper Limit
Channel Length	2.0 cm	9.0 cm
Channel Width 1	0.5 mm	1.5 mm
Channel Width 2	0.5 mm	1.5 mm
Land Width 1	1.0 mm	2.5 mm
Land Width 2	1.0 mm	2.5 mm

This section has summarized the search space of the double-serpentine optimization and has identified the necessary changes made to the Gmesh script and the GA control script when stepping from the three-parameter to the five-parameter

study. These changes resulted in an optimal configuration within the limits of the search space. It is important to point out that the optimal parameter values discussed in the following section fell within the limits set out by the GA control script. Because the optimum fell within, rather than at the extremes of any one or more of the prescribed ranges, it is evident that appropriate ranges were chosen for all five parameter values.

5.3 Comparison of Best and Worst Individuals

This discussion begins with the output of the double-serpentine optimization study. The study evaluated 130 unique individuals over a span of 15 generations beyond the initial generation. The parameters describing the best and worst individuals are summarized in Table 5.2. Comparing the best individual to other individuals in the study provides insight into the dominant physical mechanisms that govern the performance of the individuals in the search space. The influence of these mechanisms is highlighted by inspecting and comparing the individuals with the largest performance difference. Therefore, as in Chapter 4, the best and worst individuals are selected for comparison. The "worst" individual is the poorest performer identified during the optimization process, not the worst possible configuration within the limits. They are discussed in the next section.

Table 5.2: Double-Serpentine Best and Worst Individuals

Quantity or Parameter	Best	Worst
Channel Length	8.72 cm	7.79 cm
Channel Width 1	1.25 mm	1.20 mm
Channel Width 2	1.06 mm	0.99 mm
Land Width 1	1.67 mm	2.19 mm
Land Width 2	1.44 mm	1.59 mm
Net Power Density	0.694 W/m^2	0.534 W/m^2

Performing an analysis similar to Chapter 4, the following discussion identifies the physical mechanisms that govern the performance of the double-serpentine

channel configuration. Beginning on the cathode side of the cell at the CL and GDL interface, an examination of Figure 5.3 reveals that the current density of the cell is highest between adjacent channel roots. Because of the restricted area of this cell, only three double channel passes could be accommodated within the specified area with the specified lengths for both the best and worst individuals of the population. Therefore, each of these individuals has only two instances of adjacent channel roots. In the worst individual, certain regions do not produce much current due to the land width spacing of LW_1 (for example, note the blue band in the bottom of Figure 5.3). LW_1 is the width of the rib that separates the two channels that make up double-serpentine. This result is expected because as the flows proceed down channel 1 and 2 of the double-serpentine configuration from inlet to outlet, they would experience similar pressure drops, implying that the transverse pressure differential across LW_1 between channel 1 and 2 at any downstream location is small. Consequently, convective bypass is not effectively generated under the rib separating channel 1 and 2, especially when CW_1 and CW_2 have similar values.

Figure 5.3: Best (top) and worst (bottom) individuals' contour plots of current density (A/m^2) at the cathode GDL-CL interface.

The regions of poor current density indicate possible mass transport limitations resulting in reactant starvation in the CL on either side of the cell. The oxygen concentration in the GDL and the depth to which it penetrates greatly influences the current density of a given region of the cell. Figure 5.4 gives an isometric view of the oxygen concentration in the GDL of the best (top) and worst (bottom) individuals. The set of contours for each individual shows how the oxygen concentration decreases while moving from the GDL midplane to the GDL-CL interface in three planes: GDL midplane (top layer), half way between the midplane and the GDL-CL interface (middle layer), and the GDL-CL interface (bottom layer). These contour plots confirm that the wider land decreases convective bypass across the rib LW_1 during each pass. Also, the channel length of the worst individual is less than that of the best individual, meaning that in the same nominal area of the cell, the overall channel length is less. A smaller overall channel length implies a smaller total pressure drop, and so the gradient between adjacent channels is also less, and the performance therefore suffers.

The distribution of reactants in the GDL is directly influenced by the velocity, which is why it is important to next investigate the in-plane velocity vectors in the cathode GDL midplane.

In order to determine the reason for reduced reactant transport, the velocity vectors in the xz-plane are investigated on the cathode side at the GDL midplane. Figure 5.5 shows that there is less in-plane velocity between adjacent channel roots in the worst individual. A lower in-plane velocity means that there is less convective bypass, and thus, less reactant transport. Since the convective flow is proportional to the pressure difference between the channels and inversely proportional to the distance between the channels, it is therefore the geometry of the channel that causes poor performance in the worst individual. The channel configuration of the worst individual does not make efficient use of the nominal area of the cell due

to increased dead regions and therefore the net power density of the cell suffers in the worst individual. However, the best individual does make efficient use of the nominal area. This is evident from Figure 5.4 because not only is the reactant delivered evenly throughout the cell, but it also is consistently at a relatively high level. The dead zones in the cell are minimized, meaning that a large percentage of the area of the cell is producing useful current.

5.4 Comparison to Neighbors

The preceding data and discussion in this chapter have provided an explanation for the best individual's superior performance. However, this individual is the best from only a small subset of all possible individuals within the search space. As in Chapter 4, the best individual is now compared to its neighbors through a bracketing study. Assuming that the search space is relatively smooth around the optimal parameters, the bracketing study provides further evidence that the optimal individual was identified during the GA optimization. Figure 5.6 shows the results of the bracketing study conducted around the parameter values of the best individual. The adjacent individuals, or neighbors, are created by scaling each parameter by $\pm 5\%$ and $\pm 10\%$. This study resulted in 20 new individuals for whom the corresponding fitness values were evaluated.

Similar to the bracketing study of Chapter 4, none of the new individuals evaluated performed better than the best individual chosen by the GA. The neighboring individuals also showed good performance with a drop no greater than 2.75%. Referring back to Chapter 4, the neighbors of the best three-parameter individual performed to within 1.5%. This comparison shows that the neighbors surrounding the best individual are in a relatively flat operating zone, but that the five-parameter study shows a slightly steeper drop in performance when compared to the three-parameter study. This observation suggests that the PEMFC design is more sensitive to the design parameters of the study performed in this chapter.

The data discussed in this chapter give further evidence that it is important to make intelligent design decisions even within reasonable design limits. Individuals within a limited search space can perform at least 20% worse that the best individual. Isolating the channel parameters that are near the optimal value for a cell of this size with a double-serpentine configuration is therefore an important design consideration.

5.5 Comparison Between the Performance of the Best Single-Serpentine and Double-Serpentine Channel Configurations

Now that two different types of channel configurations have been optimized for PEMFC performance over the same target area, conclusions can be drawn about their respective performance. These conclusions lead not only to design parameter selection, but also to the choice of channel type for a particular PEMFC application. The fitness function in each optimization was set to maximize the net power density of the same target area. Several observations can be made by examining the current density distributions in the single- and double-serpentine channel configurations. First, the single-serpentine configuration produces an average current density across the terminal surface that is 27% greater than the double-serpentine configuration. For a cell of this size, the single-serpentine is capable of producing a higher power density despite some regions, such as the terminal passes of the anode and cathode channels, that are not producing much current due to reactant starvation. Figure 5.7 depicts the current density distribution on the cathode GDL-CL interface of the single- and double-serpentine configurations. The contour plots shows that although the double-serpentine configuration does not have any dead zones, overall, it is not producing a high amount of current. The reduced current density is directly linked to the sub-optimal distribution of reactants in the cell.

Figure 5.8 depicts the oxygen concentration along the cathode channels. The single-serpentine configuration effectively uses all of the oxygen by the time the flow

reaches the outlet of the cell. On the other hand, the double-serpentine configuration acts similarly to the worst individual in Chapter 4; the channel configuration is not effective at delivering the oxygen to the catalyst layer. Much of the reactant is therefore still present in the flow leaving at the outlet port of the cell on the cathode side. A cell's ability to deliver reactants to the CL is directly related to the convective bypass, and the lack of convective bypass is why the best double-serpentine configuration is unable to deliver the reactants to the CL.

Figure 5.9 clearly exhibits the lack of convective bypass at the root of the double-serpentine configuration. Not only are the velocities low in this region of the cell, but there are only two sets of adjacent channel roots in the entire double-serpentine cell. There is simply not enough area for the channel to make enough switchbacks. Without the switchbacks, convective bypass is greatly restricted.

The Peclet number is a dimensionless quantity that provides a relative comparison between the speed of convection and diffusion [3]. This quantity is defined in Equation 5.1 where v_z is the velocity magnitude along the z-direction, and D is the diffusivity constant. When the value of the Peclet number is greater than unity, convective transport is dominant. However, when the Peclet number is less than unity, diffusion is the dominant transport mechanism. Figures 5.10 & 5.11 show the comparison between the Peclet number for the best single- and double serpentine individuals in the cathode GDL midplanes. These figures show that convection is the dominant physical mechanism in the single-serpentine channel configuration. It is four to five times greater than the best regions in the double-serpentine channel configuration. Throughout the double-serpentine individual, diffusion is the dominant transport mechanism for oxygen transport, which reaffirms the relatively poor performance of this individual.

$$Pe = \frac{v_z LW}{\varepsilon D} \tag{5.1}$$

The pressure distribution also gives some insight into the performance of these two cells. Figure 5.12 shows the distribution of pressure in each cell. Each configuration has a different scale corresponding to the range of pressures in the respective cells. The relevant metric here is not the absolute pressures in the cell, but rather the pressure differences within each cell. The pressure difference between the inlet and outlet of the single-serpentine configuration is about three times higher than the pressure difference between the inlet and outlet of the double-serpentine individual. Since it is the pressure difference in the cell that drives convective transport, a lack of steep pressure gradients greatly limits the performance of the double-serpentine configuration.

5.6 Summary

The purpose of this chapter was to apply the GA optimization method developed for this study to a double-serpentine channel configuration in a fixed-area PEMFC. The optimal parameter values were identified and suitable evidence was presented to justify the physical behavior of the cell as well as the selection of an optimal individual. The optimal individual of this chapter was compared to the optimum single-serpentine individual within the same area constraint. It is concluded that for a fixed area of 16 cm^2, the single serpentine is significantly more effective at delivering reactants to the catalyst layer. Therefore, it is capable of producing a higher net power output and is identified as the better configuration according to the constraints imposed in these two studies. This conclusion does not imply that the single-serpentine configuration would be optimal in a PEMFC of larger nominal area. Rather, it implies that the method can be directly applied to a scaled-up area PEMFC to identify optimal parameter values for maximum performance. The next chapter presents an overall summary of the project and suggestions for future work using this thesis as a foundation.

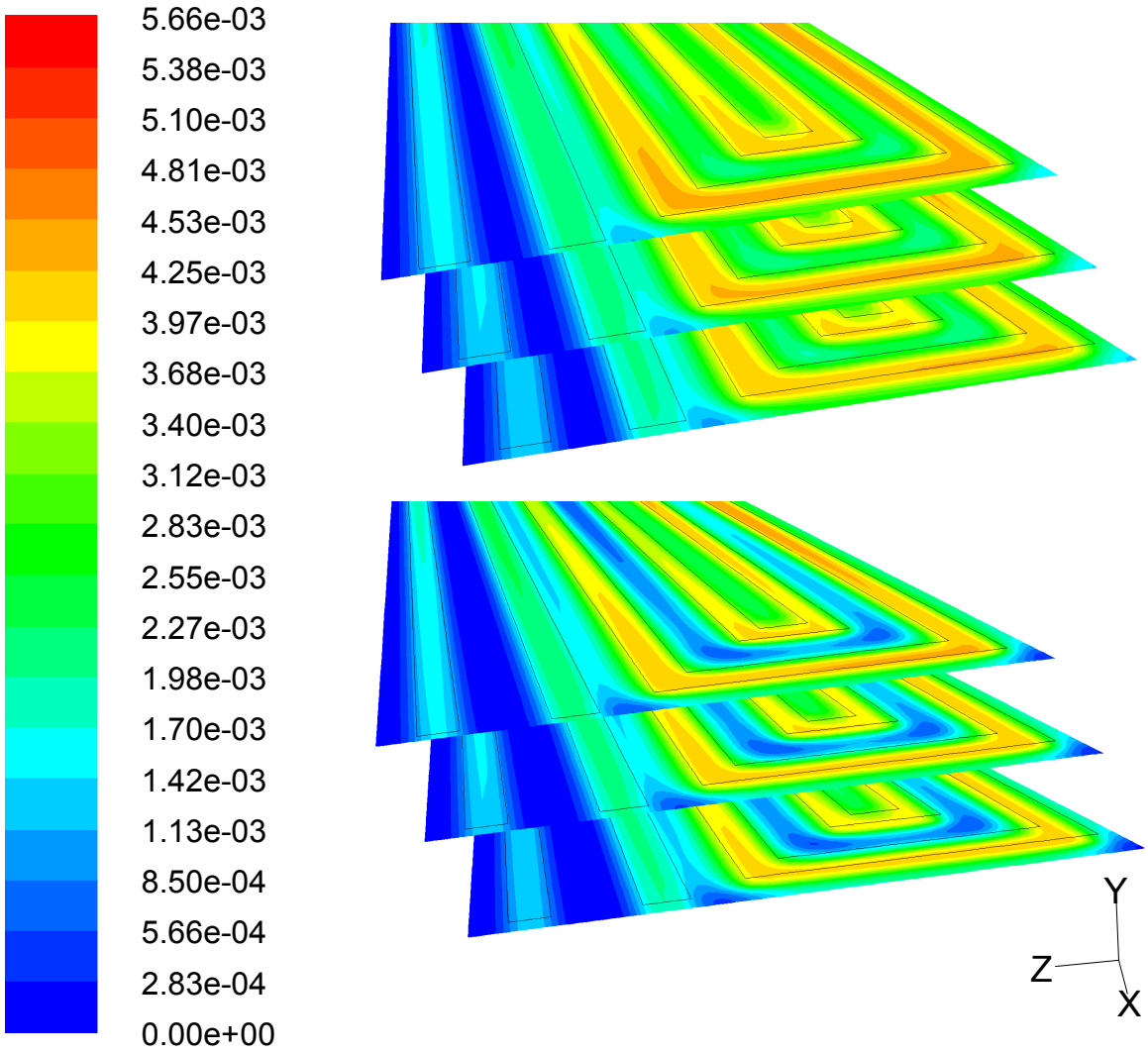

Figure 5.4: Best (top) and worst (bottom) individuals' layered contour plots of GDL molar concentration (kmol/m^3) of oxygen from the cathode GDL midplane (top) to the GDL-CL interface (bottom).

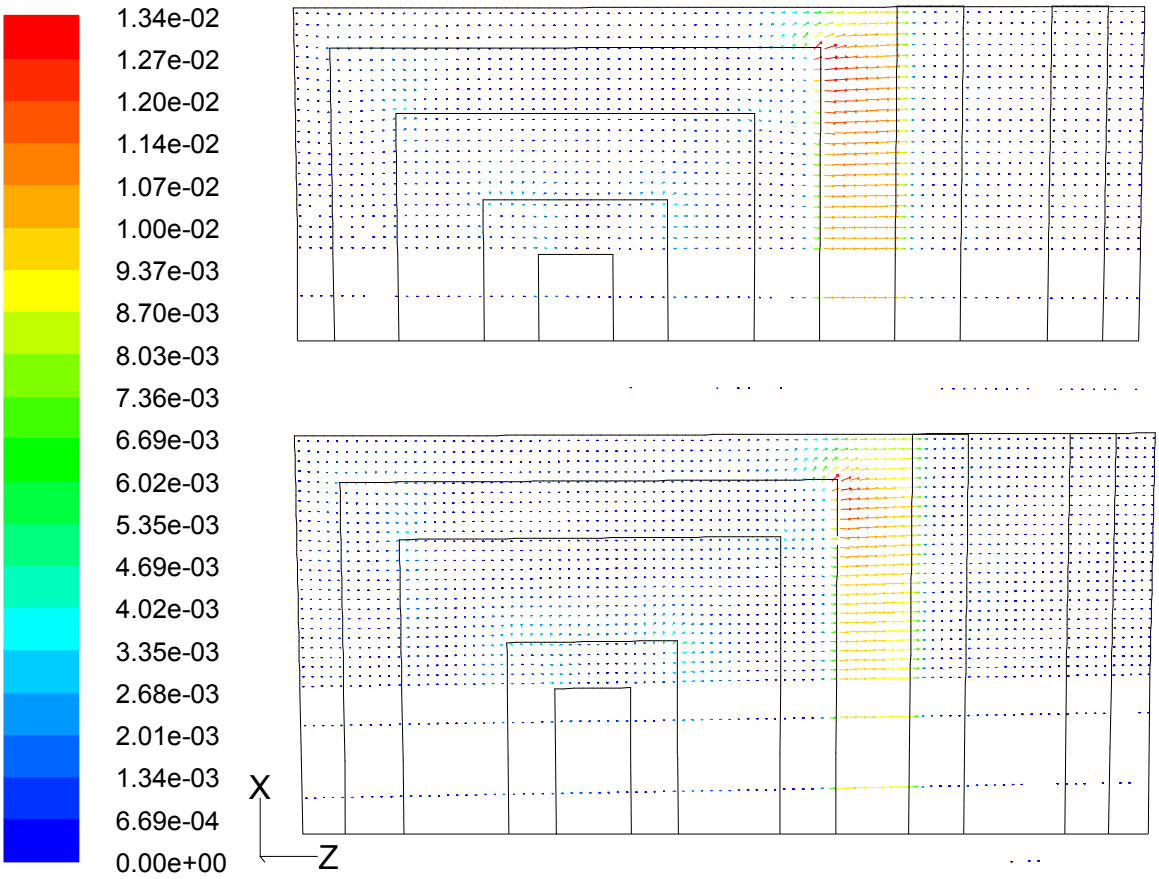

Figure 5.5: Best (top) and worst (bottom) individuals' plots of velocity (m/s) at the cathode GDL midplane.

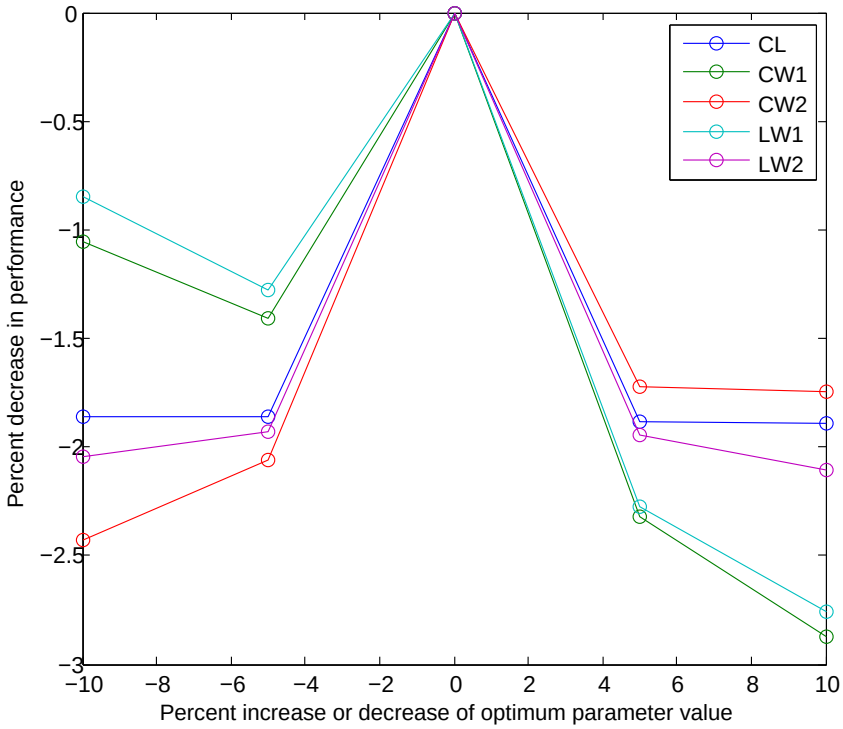

Figure 5.6: Comparison of the best double-serpentine individual's performance to that of its neighbors.

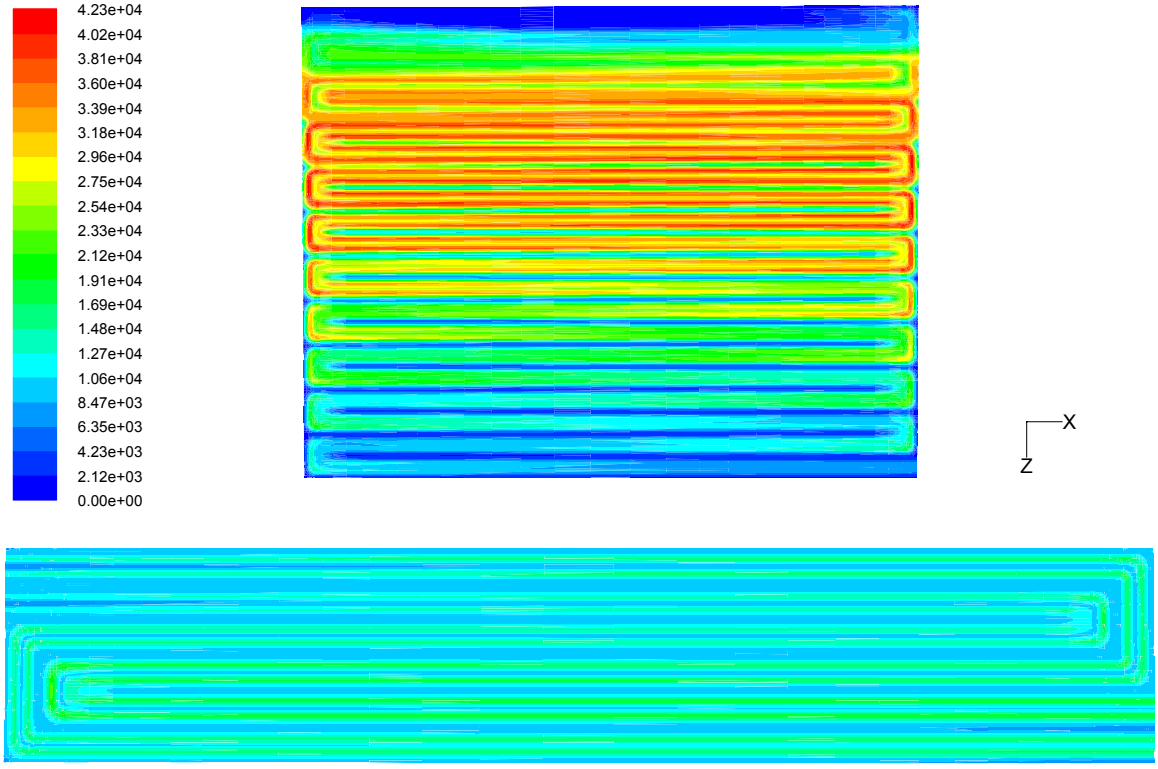

Figure 5.7: Current Density (A/m^2) contour plots at the cathode GDL-CL interface for the best single- (top) and the best double-serpentine (bottom) channel configurations.

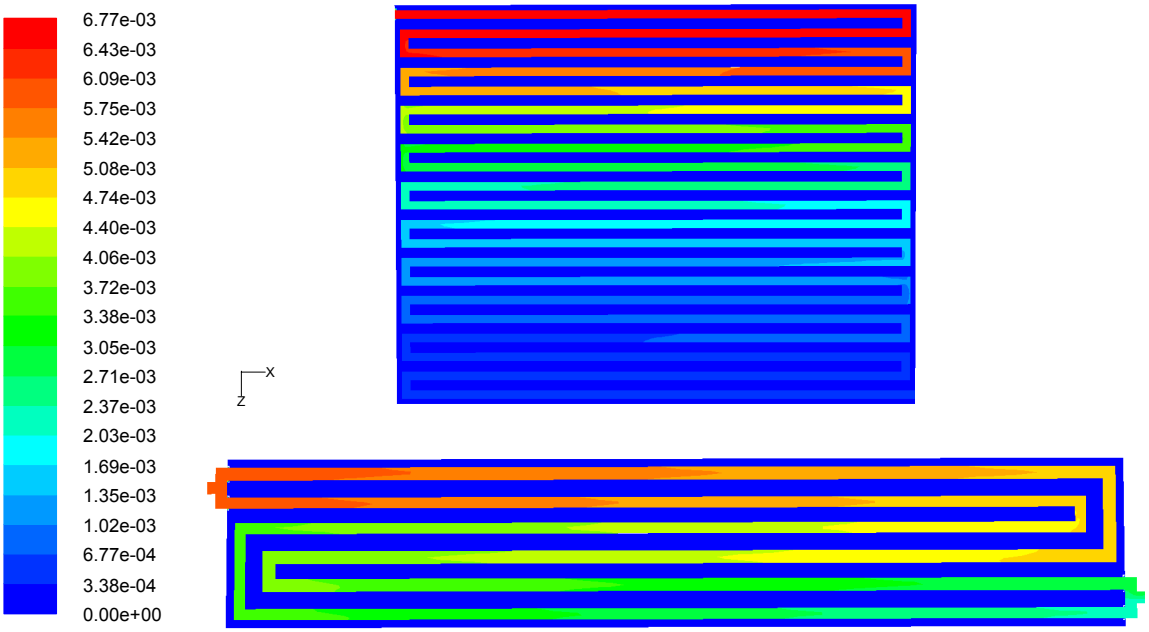

Figure 5.8: Contour plots of oxygen molar concentration (kmol/m^3) at the cathode GDL midplane for the best single- (top) and the best double-serpentine (bottom) channel configurations.

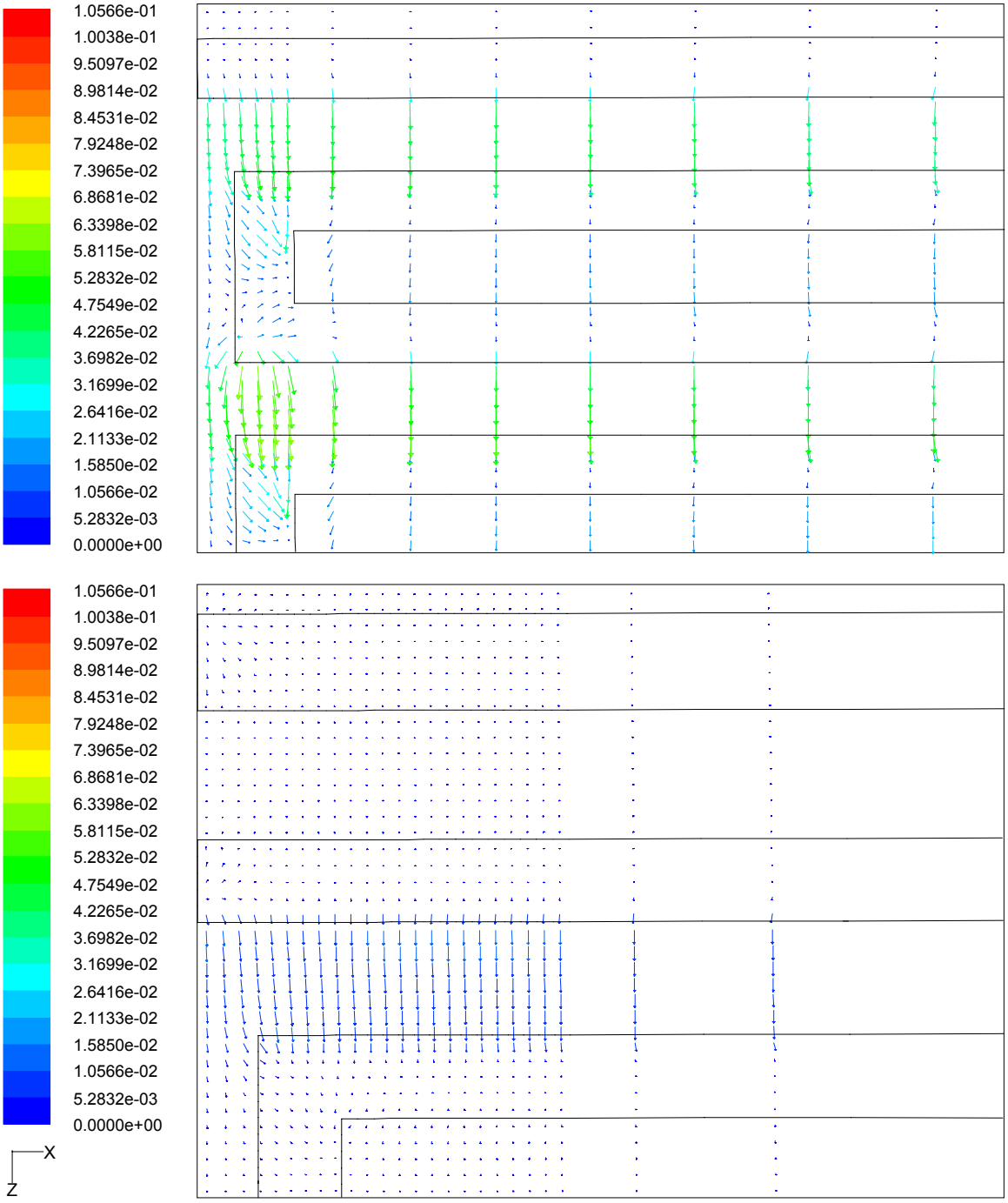

Figure 5.9: Velocity vectors (m/s) in the cathode GDL midplane for the best single- (top) and the best double-serpentine (bottom) channel configurations at adjacent channel roots.

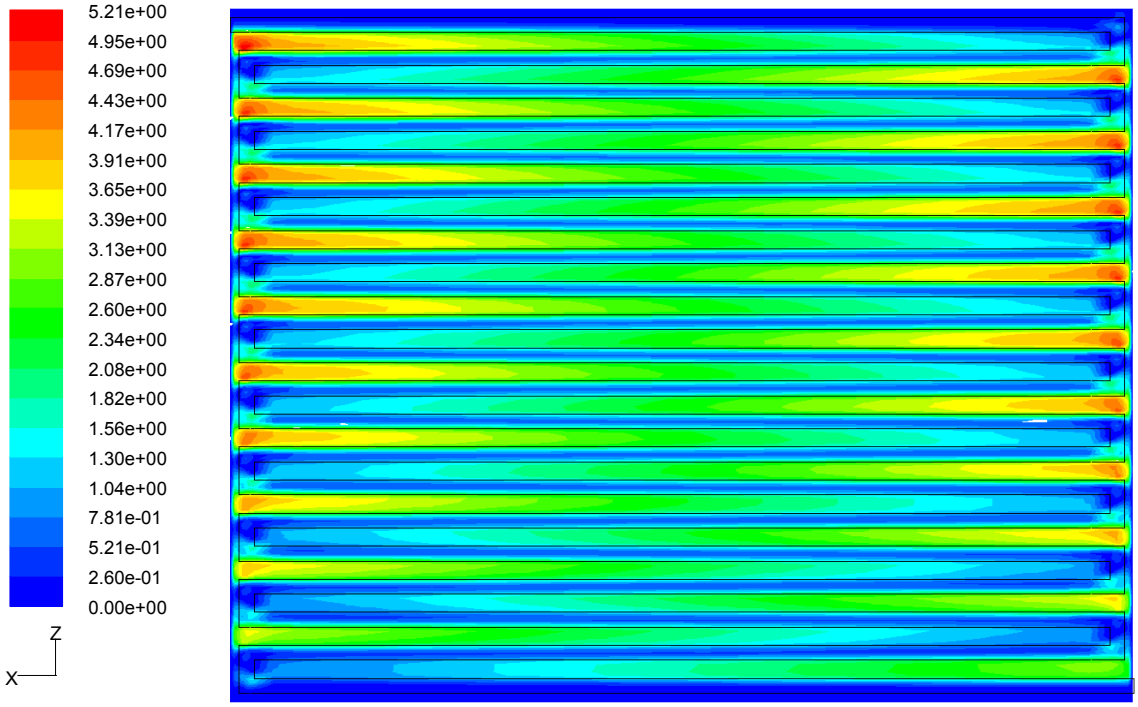

Figure 5.10: Contour plot of the Peclet number in the cathode GDL midplane of the best single-serpentine individual.

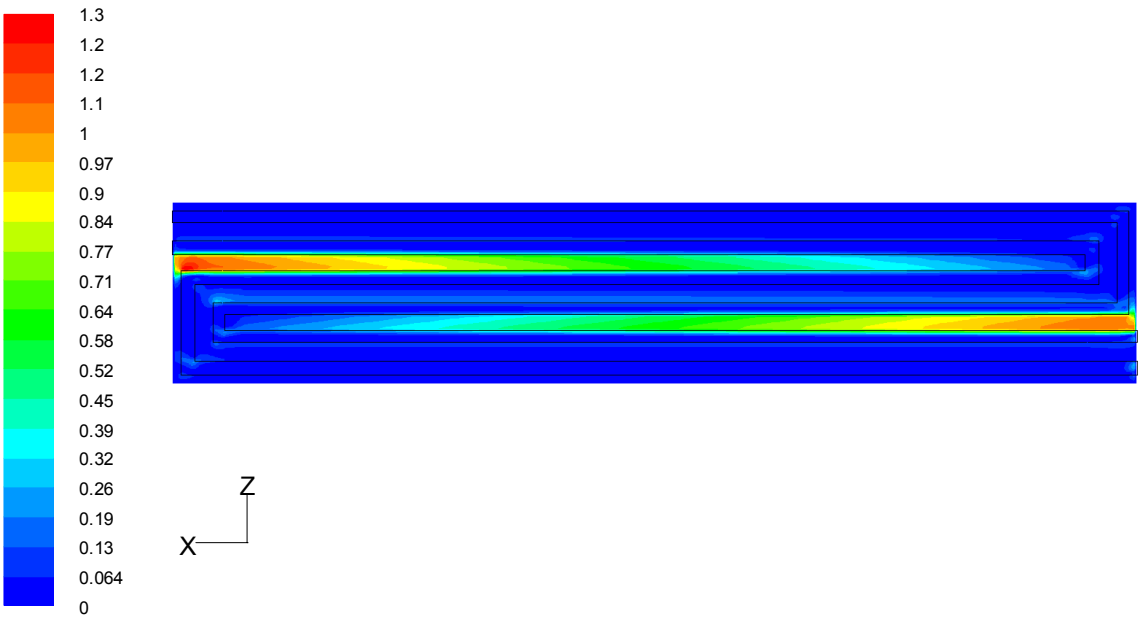

Figure 5.11: Contour plot of the Peclet number in the cathode GDL midplane of the best double-serpentine individual.

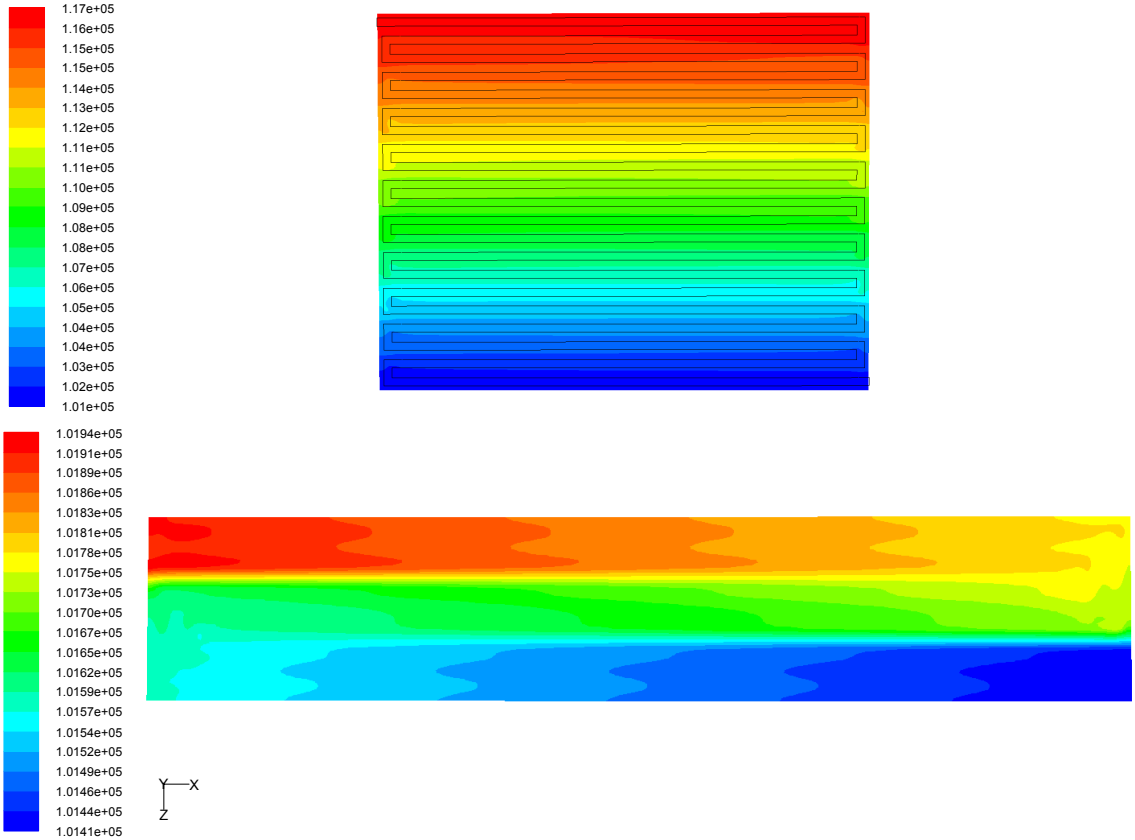

Figure 5.12: Pressure (Pa) contour plots in the cathode GDL midplane for the best single- (top) and the best double-serpentine (bottom) channel configurations.

Chapter 6

CONCLUSIONS AND FUTURE WORK

Through this research, a powerful method of incorporating the strengths of several commercially available software packages has been developed. The unique contribution of this research project is the method of efficient and automated optimization of a PEMFC for a specified application. This method has developed an interface to automate communication of inputs and outputs between GAMBIT, FLUENT, and the MatLab GA Toolbox. MatLab, GAMBIT and FLUENT each has a unique scripting language capable of producing the data flow required by the optimization process. The communication is accomplished through the combination of several scripts, written in-house, that utilize these coding languages as well as the command line.

GA optimization is a efficient tool for searching a relatively large search space for an optimal value. The search spaces associated with the single- and double-serpentine configurations of this project comprised a relatively flat solution set surrounding the neighbors in each case. Therefore, the optimization can be trusted to find an optimum relatively close to the global search space optimal value, which in each case was the net power density. This metric is useful for evaluating a PEMFC in a real world application where the cell is also responsible for powering the balance-of-plant that is required for continuous operation.

Chapter 1 focused on providing a background on fuel cell concepts as well as the motivations for investigating PEMFCs by means of numerical modeling and

simulation. Chapter 2 focused on the numerical method of simulating PEMFC performance. The performance is calculated using a commercially available software package and is meshed appropriately. Convergence criteria are discussed in this chapter as well as several types of model verification strategies. Chapter 3 provides the framework of the GA technique and the integration of the PEMFC with the various automation scripts capable of parameterizing the flow field configurations. Chapter 4 is a case study that optimizes the single-serpentine channel parameter values for maximum performance of a PEMFC for a given area. Chapter 5 extends the study of the previous chapter to an increased search space that describes a double-serpentine channel configuration. The optimal values are identified for each of the channel types and the physical mechanisms that explain the levels of performance are discussed in detail. Evidence is also provided in these chapters to help bring confidence that the optimal individuals selected during the optimization process are also globally maximum individuals.

Known limitations of this project include, but are not limited to several important considerations. First, the PEMFC model employed here assumed single-phase flow, which in reality, is incorrect. The production and transport of liquid water on the cathode, including flooding, is highly relevant for PEMFC performance characterization. Flooding can have a dramatic effect on the reactant gas flow in the cell both in the GDL and in the channel. Multiphase flow was not considered in this PEMFC model in order to reduce model complexity and computational time. Second, the best individuals tended to consume all of the available reactants before reaching the outlet ports of the cell implying some degree of reactant starvation. These cells could have benefited from a higher inlet mass flow rate such that the reactant utilization was not quite so high, as long as the increased pumping power did not cause the net power density of the cell to drop.

While the search spaces explored by this algorithm thus far are useful for

lab-scale fuel cell evaluation and comparison, the real value is in the optimization's ability to find an optimal PEMFC design configuration of any size. By successfully demonstrating the optimization of laboratory-scale PEMFCs, the method can confidently be applied to fuel cells of a larger target area. It is expected that in cells with a larger area, the physical mechanisms that govern PEMFC performance would find different optimal parameter values. The method developed here is capable of including as many parameters as a user desires, including varying the material properties. Such additional parameters may include, but are not limited to: channel height, GDL thickness, GDL porosity, GDL permeability, channel taper, and the number of serpentine channels in parallel.

A significant feature of the method developed by this research project is that other types of flow fields can also be evaluated. Configurations such as parallel, interdigitated, and multiple serpentine channels can be incorporated using the Gmesh script developed for this study. As long as the same zones and boundary condition types are prescribed by the Gmesh script, the Fjou script is capable of evaluating the fitness of any PEMFC and its desired channel configuration. However, it is recommended that mesh refinement studies are conducted on new channel configurations to ensure proper convergence and solution accuracy.

Future applications of this search algorithm can include multi-objective optimizations. The optimizations performed in this project searched for the optimum set of values at a specific operating voltage and operating conditions. However, a PEMFC may be desired to perform optimally under a variety of operating conditions. Therefore, the fitness function can be adapted to evaluate the performance of an individual at several different operating conditions and define fitness as an individual's ability to perform well for all conditions of interest.

Another possible application of this method is to design a completely randomized flow field. The flow field can be broken down into a grid of voxels. Turning

one voxel on would mean that it is a fixed height flow channel segment, and turning one off would mean that it is filled by the bipolar plate material to create a land region. Whether a particular voxel is turned on or off would constitute an independent design parameter. The finer the grid, the greater the number of independent design parameters the GA would require. The fitness (for example, the net power density) of the individuals would be evaluated and a new type of channel that runs an efficient fuel cell could emerge. The current Fjou script can handle such a scenario, as long as an appropriate Gmesh script is developed. The GA control script would require modification to contain the appropriate number of design parameters and the limits set on each of them. The large search space that this would encompass requires many more generations and individuals. This scale of optimization would greatly benefit from a parallel calculation of fitness, and larger computational resources than those used in this project. The current limitation is due to the huge computation time required by the fuel cell module to run in FLUENT.

A final, more general application of the method developed in this project is to use the framework of communication between software packages to optimize other types of engineering optimization problems. With the appropriately defined Gmesh and Fjou scripts and fitness functions, the communication scripts can be adapted to any problem capable of FEA modeling. However, any final output should always be carefully analyzed for physically accurate and sensible results. Ideally, a necessary step in the overall design of any device should include a validation of the predicted results.

BIBLIOGRAPHY

[1] Falin Chen, Ying-Zhi Wen, Hsin-Sen Chu, Wei-Mon Yan, and Chyi-Yeou Soong. Convenient two-dimensional model for design of fuel channels for proton exchange membrane fuel cells. *Journal of Power Sources*, 128(2):125 – 134, 2004.

[2] J.P. Feser, A.K. Prasad, and S.G. Advani. Experimental characterization of in-plane permeability of gas diffusion layers. *Journal of Power Sources*, 162(2):1226 – 1231, 2006. Special issue including selected papers from the International Power Sources Symposium 2005 together with regular papers.

[3] J.P. Feser, A.K. Prasad, and S.G. Advani. On the relative influence of convection in serpentine flow fields of pem fuel cells. *Journal of Power Sources*, 161(1):404 – 412, 2006.

[4] Guilin Hu, Jianren Fan, Song Chen, Yongjiang Liu, and Kefa Cen. Three-dimensional numerical analysis of proton exchange membrane fuel cells (pemfcs) with conventional and interdigitated flow fields. *Journal of Power Sources*, 136(1):1 – 9, 2004.

[5] Fluent Inc. *User's guide for GAMBIT Version 2.4.6.* Fluent Inc., 2000.

[6] Fluent Inc. *User's guide for FLUENT Version 6.3.26.* Fluent Inc., 2006.

[7] D.H. Jeon, S. Greenway, S. Shimpalee, and J.W. Van Zee. The effect of serpentine flow-field designs on pem fuel cell performance. *International Journal of Hydrogen Energy*, 33(3):1052 – 1066, 2008.

[8] J. Larminie and A. Dicks. *Fuel Cell Systems Explained*. Wiley, 2003.

[9] Anh Dinh Le and Biao Zhou. A general model of proton exchange membrane fuel cell. *Journal of Power Sources*, 182(1):197 – 222, 2008.

[10] H.C. Liu, W.M. Yan, C.Y. Soong, Falin Chen, and H.S. Chu. Reactant gas transport and cell performance of proton exchange membrane fuel cells with tapered flow field design. *Journal of Power Sources*, 158(1):78 – 87, 2006.

[11] J.G. Pharoah. On the permeability of gas diffusion media used in pem fuel cells. *Journal of Power Sources*, 144(1):77 – 82, 2005.

[12] S.N. Sivanandam and S.N. Deepa. *Introduction to Genetic Algorithms*. Springer, 2007.

[13] Dusan Spernjak, Ajay K. Prasad, and Suresh G. Advani. Experimental investigation of liquid water formation and transport in a transparent single-serpentine pem fuel cell. *Journal of Power Sources*, 170(2):334 – 344, 2007.

[14] S. Gottesfeld T.E. Springer, T.A. Zawodzinski. Polymer electrolyte fuel cell model. *J. Electrochemical Society*, 138(8):2334 – 2342, 1991.

[15] C.Y. Wang Sukkee Um and K.S. Chen. Computational fluid dynamics modeling of proton exchange membrane fuel cells. *J. Electrochemical Society*, 147(12):4485 – 4493, 2000.

[16] Xiao-Dong Wang, Yuan-Yuan Duan, and Wei-Mon Yan. Numerical study of cell performance and local transport phenomena in pem fuel cells with various flow channel area ratios. *Journal of Power Sources*, 172(1):265 – 277, 2007. ACS San Francisco 2006, Fuel and Cell Symposium. American Chemical Society National Meeting. San Francisco, CA Sept 10-14 2006.

[17] C. Xu and T.S. Zhao. A new flow field design for polymer electrolyte-based fuel cells. *Electrochemistry Communications*, 9(3):497 – 503, 2007.